iScience

CellPress
OPEN ACCESS

Review

Igneous processes in the small bodies of the Solar System II: Small satellites and dwarf planets

Giovanni Leone[1,2,5,*] and Hiroyuki Tanaka[2,3,4]

SUMMARY

Evidence of hot and cold igneous processes has been reported in small satellites and dwarf planets of the Solar System. Olivine and pyroxenes were detected in the spectral bands of both small satellites and dwarf planets. The aqueously altered form of olivine and serpentine has been detected in the spectrums of Ceres and Miranda hinting at possible hydrothermal processes in their interiors. Once more, the ubiquitous distribution of ^{26}Al in the planetary nebula, then evolving in the protoplanetary disk, contributed to the primordial widespread heating. Volcanism, or cryovolcanism, then developed only in those bodies where long-lived radiogenic elements, and/or tidal processes, were available.

INTRODUCTION

Following the previous work by Leone and Tanaka[1] in which the igneous processes in asteroids and comets were reviewed, we have focused this work on the small satellites and dwarf planets of the Solar System that are still quite underrepresented in the available literature. We deem those bodies like Io and Enceladus have already been well covered also thanks to dedicated missions like Galileo and Cassini, but other small bodies have not received the same attention even though some spacecraft or ground-based data are available. Once again, we distinguish igneous processes from volcanism, the former being not specifically associated with eruptive activity but merely with heating.[1] Thus, igneous processes can be caused by any source that is able to produce heat. The typical heating sources present at the beginning of the history of our Solar System were already discussed in the previous paper (Leone and Tanaka[1]), but we will briefly resume them here as well: impact, accretion and differentiation, tidal interaction (where available), and radiogenic decay. These heating sources have contributed to generate igneous processes in various small bodies of the Solar System but not volcanism everywhere. For example, volcanism is currently ongoing on Io because tidally fed eruptive activity is observed whereas only igneous processes have been postulated on Amalthea[2] because the products of volcanism (i.e., lava flows) have not been observed on its surface. Olivine, one of the typical minerals present in lava, has been spectroscopically detected on Amalthea in its unaltered form.[3–5] Serpentine (its aqueous altered form) was directly detected on Ceres[6] and Miranda.[7] Olivine was assumed to be present in the modeling of Charon's,[8,9] Deimos', and Phobos'[10] formation. At last, the possible presence of olivine was inferred in Haumea's[11] and Sedna's[12] interiors from theoretical modeling. We have already seen in the previous work by Leone and Tanaka[1] that the presence of olivine alone is not the "smoking gun" for past igneous and/or volcanic processes, as it could be recycled from the interstellar medium (ISM), but if it is present combined with the suite of minerals typical of igneous rocks (i.e., pyroxenes, feldspars) with the possible presence of volcanic features or lava flows, well, then it becomes a possible evidence in such a case. Igneous processes have also been postulated during the formation of Deimos and Phobos,[10] while possible cryovolcanism on Charon,[13] Miranda,[14,15] 120347 Salacia and Orcus,[16] Quaoar,[17] and Sedna[12] has been reported. Ceres is the only small body of the Solar System in which evidence of both volcanism[18] and possible cryovolcanism[19] is shown.

Cryovolcanism is somehow the cold version of volcanism, and it was quite common in the outer Solar System. The difference with hot volcanism is that cryomagma, usually a mixture of water and ammonia (acting as "antifreeze"), does not rise alone to the surface as well as magma in diapirs because water is denser than ice.[20] It is true that magma may also stall in deep or shallow reservoirs once it reaches the same density of the host rock, but the processes of differentiation (or entrainment of volatiles during the rise) lower the density of magma so that it can start its rise again to the surface. The same convention used for lava also applies for cryolava; it is called cryomagma when it is still underground, and it is called cryolava when it is erupted onto the surface. Enceladus, and possibly Europa,[21] are the bodies in which cryovolcanism is currently ongoing. We do not know if cryovolcanism is currently ongoing in the distant dwarf planets not yet reached by a spacecraft, but there are signs that may indicate some activity on Quaoar.[8,22] Enceladus is an example in the Solar System in which concentrations of long-lived radiogenic elements may still feed its cryovolcanic activity in addition to the tidal heating from Saturn.[23]

[1]Instituto de Investigación en Astronomía y Ciencias Planetarias, Universidad de Atacama, Copiapó 153000, Región de Atacama, Chile
[2]Virtual Muography Institute, Global, Tokyo, Japan
[3]International Muography Research Organization (MUOGRAPHIX), The University of Tokyo, Tokyo, Japan
[4]Earthquake Research Institute, The University of Tokyo, 1-1-1 Yayoi, Bunkyo, Tokyo 113 -0032, Japan
[5]Present address: Instituto de Investigación en Astronomía y Ciencias Planetarias, Universidad de Atacama, Copiapó, Chile
*Correspondence: giovanni.leone@uda.cl
https://doi.org/10.1016/j.isci.2024.109613

NATURE OF CRYOVOLCANISM

Cryovolcanism was defined as "the extrusion of liquids and vapors of materials that would be frozen solid at the planetary surface temperatures of the icy bodies of the outer solar system."[24] Usually, this extrusion has been observed in form of geysers on Enceladus[25] although cryomagmas erupted onto the cold surfaces of the outer Solar System satellites and dwarf planets become cryolavas and behave rheologically like silicate lavas forming solid crusts and flow fronts, carving channels, and forming all those geomorphological features typical of erosion like chaos, colles, etc … The result is a wide variety of geomorphological features similar to the surfaces of the rocky planets and satellites of the inner Solar System.

Of course, both magma and cryomagma need to rise to the surface to form extrusions, or even intrusions if freezing occurs into the solid crust, and the main principle that they have in common is the density difference with the host rock, or ice crust, that rules the rise. In the case of cryovolcanism, the increase of ice density at depth may help the rise of cryomagmas as far as buoyancy level is attained, but then pressurization is needed, and different mechanisms for the final rise to the surface have been proposed: a) freezing of an ammonia-ice mixture in a cryomagma reservoir, which generates an overpressure exerting an extensional stress that fractures the reservoir's wall creating a crack through which cryomagma can escape[20]; b) exsolution of volatiles (i.e., CO_2, CO, CH_4, SO_2) creating an overpressure at the crack tip over the reservoir[26]; c) intrusion of silicate magma at the base of the ice crust with melting and mobilization of cryomagma[27]; d) topographically driven flow into low-lying regions[28]; e) shear heating by tidally driven lateral (strike-slip) fault motion[29]; and f) tidally driven stress forming fractures and additional stress at depth due to the overburden pressure.[30]

For brevity we do not enter into much detail of the various mechanisms in this work, and we suggest to read the aforementioned literature. However, we notice a point in common among all these mechanisms. Although only some of these mechanisms involve direct heating, the availability of liquid water in other mechanisms also requires a previous heat source for the melting of ice crust and the formation of water reservoirs or even subsurface oceans. So, whatever is the heat source involved (tidal or radiogenic or both), igneous processes are at the basis of both volcanism and cryovolcanism albeit with obvious different temperatures. This is exactly what we will see in the following sections.

BORDER BETWEEN "HOT" VOLCANISM AND "COLD" (CRYO-)VOLCANISM

Evidence of past "hot" volcanic processes outside the Earth, in which direct eruption of hot lava on the surface is observable, has been found on the Moon, Mars, Mercury, and Venus. Both lava and pyroclastic eruptions, including magmatic crustal intrusions, have been postulated on 4 Vesta.[31] Direct evidence for lava flows on the ground was not found in Dawn images.[32] However, the discovery of unexpected olivine-rich craters on 4 Vesta suggests that direct eruption of magma from the mantle to the surface may have indeed occurred.[33] Evidence of ongoing volcanic eruptions has been found on Io[34] and suggested for Venus[35,36], but from Ceres onwards to the outer Solar System there is widespread evidence of cryovolcanism. However, the evidence of cryovolcanism on Ceres still remains elusive[37] while it is directly observed on Enceladus through its geysers and rejuvenation of the surface in its southern hemisphere.[38]

Based on these observations, we might place the border between hot volcanism and cold (cryo-)volcanism between the orbits of Io and Europa. But the "artificial" nature of Io's hot volcanism, being pumped up by the tidal heating of Jupiter,[39] does not make it a good candidate for internally heated volcanism (i.e., generated solely by internal radioactive decay). A radiogenic contribution to its heat flow might be possible, but the distribution of the heat flow is not globally uniform[40] thus suggesting that its main fraction might be tidal. The tidal heating of Europa by Jupiter is not enough to generate hot volcanism but at least prevented Europa from total freezing.[41] On the other hand, evidence of sporadic plume activity has been found on Europa.[21] It could be objected that also Enceladus could be regarded as a tidally powered world, but new calculations showed how the main fraction of its heat flow is not tidal.[23] In such a case, the border should be moved back to the asteroid belt (henceforth AB) between 4 Vesta and Ceres roughly between 2.36 and 2.76 astronomical unit (au) from the Sun (Figure 1). Interestingly, the "frost (or snow) line," that is, the distance from the Sun where the low temperatures force a volatile molecule to form ice particles, is placed beyond the orbit of Mars (1.52 au)[24,42] to just little less than 5 au.[43] On average, considering the upper and lower limits, the snow line could be centered at ~3.21–3.25 au. Basically, the border between hot volcanism and cryovolcanism is placed just in the middle of the range suggested for the frost line (Figure 1).

IGNEOUS PROCESSES IN SMALL SATELLITES OF THE SOLAR SYSTEM

In the past years much attention has been drawn by active satellites of Jupiter and Saturn, Io and Enceladus, also thanks to dedicated missions like Galileo and Cassini. However, other small satellites of the Solar System were characterized by igneous processes in the past although they appear not active anymore. As we have seen with asteroids, due to the widespread distribution of ^{26}Al[1] in the protoplanetary disk, almost every small body of the Solar System has been characterized by igneous processes at the initial time of its earliest formation. We will explore the thermal processes of the underrepresented small satellites and dwarf planets. We also will explore whether these thermal processes can reach temperatures high enough to melt mafic minerals like pyroxenes and/or olivine. Cryovolcanism, as a thermal process that has characterized many small bodies of the Solar System, will be discussed in comparison to "hot" volcanism in the discussion section.

Amalthea

Amalthea is an irregularly shaped (270 × 165 × 150 km) satellite of Jupiter showing a surface composition similar to that of C-type asteroids, D-type,[5] or Deimos and Phobos with patches of very red material interpreted as sulfur and sulfur compounds[44,45] likely coming from the volcanic activity of the nearby satellite Io.[46] Various hypotheses have been suggested for the formation of Amalthea.

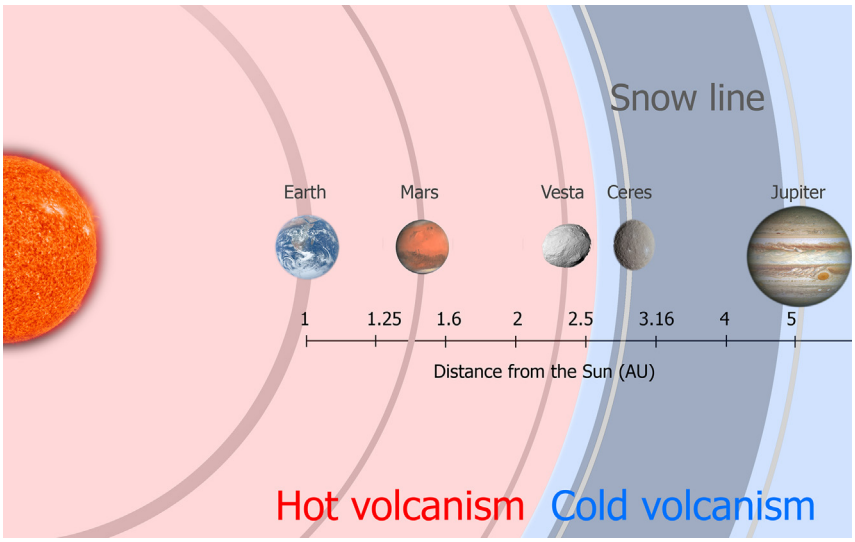

Figure 1. Border between hot and cold (cryo-)volcanism (red and blue regions, respectively) located between the orbits of 4 Vesta and Ceres
The gray area corresponds to the "frost or snow" line placed between 2.7 and 4.9 au of distance from the Sun. Size of the bodies not to scale.

According to Cameron and Pollack[2] the temperature of the region near 2.55 R_J may have ranged from 500 to 1,400 K, depending on the opacity of the proto-Jovian nebula, with the lower end (500 K) producing more silicate-rich materials similar to those found in chondritic meteorites and the upper end (1,400 K) resulting in more rocky, highly refractory, materials. Alternatively, Pollack et al.[47] proposed a formation as carbonaceous asteroid captured through a gas-drag mechanism. The hypothesis of the capture was also suggested by the similarity in size and composition with the Trojans asteroids, and Hektor in particular shows magnesium-rich pyroxene (Mg, Fe SiO_3).[48] The mean density of Amalthea was proposed as an eventual distinctive method to evaluate its origin; an average density >3.0 g cm^{-3} would suggest formation in place while <2.5 g cm^{-3} would suggest a capture.[45] This range, however, leaves an interpretational void for average densities between 2.5 and 3.0 g cm^{-3}. To resume, the low inclination and eccentricity of the orbit of Amalthea have led to think that it formed around Jupiter, but its low bulk density (due to mostly water ice in its composition) is inconsistent with the temperature in the original circum-Jovian nebula and thus comes the hypothesis of the capture from its original position closer to Callisto.[5]

During the 90's, the mapping work of Stooke[46] gave an adjustment to the shape of Amalthea; the axes were corrected to 270 km, 140 km, and 122 km, respectively, but it did not give significant information about the overall surface composition. Only with the flyby of the Galileo spacecraft, the first measurements of Amalthea's mass ($2.08 \pm 0.15 \times 10^{18}$ kg) and density (857 ± 99 kg m^{-3}) gave the first insight on a possible composition by water ice mixed with rocky material implying that the satellite was formed away from Jupiter's environment, characterized by temperatures too high for the stability of water ice, and then captured to its current position.[49]

Later, astrometric observations of Amalthea (and Thebe) made with the Cassini spacecraft essentially confirmed previous conclusions drawn by Ockert-Bell et al.[50] by which Amalthea (and Thebe) may have been sources of Jupiter's ring materials.[51] Voyager 1 and 2, Galileo, Cassini, New Horizons, and also telescopes in space (Hubble) and from the Earth (Keck) observed electrostatic lofting of dust from Amalthea into the gossamer ring of Jupiter (i.e., Borisov et al.[52] and references therein).

Further observations found a spectral similarity between the composition of the main ring of Jupiter and the surface of Amalthea, consistent with pyroxene/olivine bands seen in asteroids,[3–5] thus raising the possibility that Amalthea may have had some igneous processes that formed the observed pyroxene/olivine. However, these observations draw us back to the particular problem in existing models of formation of the Galilean satellites by a process of condensation and accretion from the circum-Jovian nebula.[53,54]

Why are Amalthea, Ganymede, and Callisto, which are the innermost (Amalthea) and outermost (Ganymede and Callisto) Galilean satellites, respectively, the iciest compositions? A possible explanation is that all the Galilean satellites formed with large icy components but later only Io were characterized by sufficient heating to drive most of the water off their bodies.[55] Long-lived radiogenic and tidal heating was thought to be negligible for Amalthea[56] as well as magnetic induction heating.[57] Thus, the only possible explanation for the observed pyroxene/olivine bands is an initial entrainment during its formation, maybe heated due to short-lived radiogenic elements, which soon exhausted according to the known[58] half-life of ^{26}Al for example. This means that the internal heat of Amalthea may have ceased 7.05×10^5 years $\pm$ 3.4% after calcium - aluminum inclusions (CAI).

Charon

Charon, with a radius of 606 $\pm$ 0.5 km and an average bulk density of 1,702 $\pm$ 17 kg m^{-3} [59] or 1,701 $\pm$ 33 kg m^{-3}, [60] is the main moon of Pluto. The lower density of Charon with respect to Pluto (1,854 $\pm$ 11 kg m^{-3}) implies that it must have a lower silicate fraction.[60] The surface of Charon exhibits a variety of geomorphological features among which are a few km-high mountains that cross the landscape from the

southwest to the northeast of the planisphere. Emblematic is the case of Kubrick Mons, a conical mountain of 34 km in diameter and 3–4 km high, which has been interpreted as emplaced by cryovolcanism.[13]

In the evaluation between a "hot" and "cold" start model for both Pluto and Charon, Bierson et al.[61] explain that extensional stress on an icy planetary body would be associated to a hot start; the ice shell thickens rapidly due to heat conduction exceeding radioactive heat production, and such extensional stress was interpreted through the observation of chasmata features on Charon's surface.[13] However, a word of caution is always recommendable before interpreting tectonic features from geomorphology alone because chasmata on Mars revealed to be erosional features rather than tectonic features[62] and cryolava is able to produce its own erosional features (i.e., cryolava channels) as seen on Titan.[63]

In absence of significant tidal heating for Charon,[64] the formation of crystalline ice and of the smooth plains observed on its surface suggests cryovolcanic processes that must have been generated by radiogenic decay in a 420 km rocky core representative of olivine (or 463 km of serpentine) composition.[8,9] Another way to form crystalline ice on the surface of Charon is by vaporization and subsequent recondensation after micrometeoroid impact.[65,66] It is not clear whether the initial phase of orbital synchronization with Pluto might have generated sufficient tidal heating to warm up Charon significantly. Barr and Collins[67] suggested a strong tidal heating, but Malamud et al.[68] opted for a formation model in which the following heat sources are considered: radiogenic heating, latent heat released/absorbed by geochemical reactions, surface insolation, gravitational energy associated with internal redistribution of mass and/or size change, and latent heat of crystallization of amorphous ice; additional improvements with respect to previous models[16] include serpentine dehydration and non-constant solar illumination.

In the Malamud et al.[68] model, Charon is approximated as a spherical body. The results of this model show that the evolution of Charon went through five steps characterized by alternate decrease and increase in radius' size: 1) an initial phase between 0 and 137 Ma in which the temperature was still below the melting point of water and there was a global radius decrease due to compaction of the ice shell; 2) between 137 and 164 Ma the melting temperature of water was internally reached with a rapid release of energy from the serpentinization of the rock, and the underlying mantle layers were fully hydrated with exception of the outermost layers where the temperature was still too cold for the melting of water; 3) between 164 and 450 Ma the differentiation by liquid water started in the previous step continues and the remaining free water freezes at the base of the mantle thus increasing its thickness and the overall Charon's size, and the core now devoid of ice increases its temperature due to radiogenic heating; 4) between 450 and 1,000 Ma the internal temperature of Charon rose to 450 K, core compaction starts as a result of self-gravity, and the overall radius of Charon decreases; 5) between 1,000 and 4,600 Ma the core temperature reached 675 K and the central part of Charon loses the water previously absorbed thus becoming dehydrated, and by the end of the evolution at 4,600 Ma the released water migrates to the base of the mantle and freezes with a further decrease of Charon's size.[68]

The thermal evolution of Charon was also reconstructed through another model after its origin from a circumplutonian disk of debris formed by a possible giant impact between two progenitor bodies of ≈1,000 km of radius (964 km and 981.6 km, respectively) occurred in the Pluto system in a 0.1–0.5 Ga interval of time after CAI.[13] The hypothesis of an impact with Pluto was suggested by Stern[69] in a review of the Pluto-Charon system. Later this hypothesis evolved in a collision between two undifferentiated (70% and 30%, respectively, of the Pluto-Charon mass) or two differentiated (50%-50% of the Pluto-Charon mass) progenitor bodies.[70] Following the hypothesis of Stern,[69] Canup[70] suggested an external impactor colliding with Pluto to form Charon. As Canup explained, "a more promising scenario involves the collision of Pluto and an impactor both already trapped in the 3:2, as in this case, a lower relative velocity due to the difference in their forced and/or free eccentricities could result, and the post-impact pair might then remain in resonance."[70] In this case, the key factor is a low-velocity impact to avoid dislodging Pluto from resonance and two possibilities exist: one is that the impact occurred when the Pluto-Charon system was already captured by Neptune and another is that it occurred before. This scenario lends toward oblique low-velocity impacts which were suggested to be common in binary systems like the Earth-Moon as well.[71] In their model of Charon's formation by collision between Pluto and an impactor one-third of its mass, Sekine et al.[72] set the impact velocity at ≈ 1 km s^{-1} with an initial temperature for proto-Pluto around 150–200 K. However, other authors think that such impacts are rare and suggested smaller impacts producing smaller and coevolving satellites.[73] The discovery of other moons, Nix and Hydra,[74] and Styx and Kerberos (i.e., Barr et al.[67] and references therein), in the same resonance of Charon with Pluto strengthened the hypothesis of formation from post-giant impact debris.[75–77]

A key factor of the thermal evolution through this other model is the fraction of rock annealed in the ice: with 0.75% of rock freezing occurs 2.8 Ga after CAI at 0.1 Ga impact time or 3.0 Ga at 0.5 Ga impact time; with 58% of rock annealed in the ice, freezing occurs at 4.0 Ga no matter whether the impact occurs at 0.1 or 0.5 Ga.[13] The complete methodology used in this other model for the formation of the Pluto-Charon system is available in Desch and Neveu.[13] For brevity here we mention only the key equation referring to the parameterization used and its basic assumptions. The progenitors must be differentiated to a radius that is called R_{diff}:

$$R_{diff} = \left(\frac{\rho_{pl} - \rho_{fi}}{2(\rho - \rho_{fi})}\right)^{\frac{1}{3}} R_{pl} \quad \text{(Equation 1)}$$

where ρ_{pl} = 1,860 kg m^{-3} and R_{pl} = 1,187 km are the density and radius of Pluto, respectively, ρ_{fi} is the density of the rocky fractions, and ρ is the starting density of the two colliding undifferentiated progenitor bodies that then differentiate to R_{diff}. In order to reproduce the Pluto and Charon system R_{diff} will be 964 km for 58% of rock and 981.6 km for 0.75% of rock.

Deimos and Phobos

Deimos and Phobos are the moons of Mars. Their respective average radii are 6.12 km[78] and 10.7 km,[79] and their respective average bulk densities are ≈1.48 and 1.876 g cm^{-3}.[80] The latter value of 1.876 g cm^{-3} is an adjustment with respect to previous Viking measurements in which both satellites were assessed having essentially the same density of 1.9–2.0 ± 0.6 g cm^{-3}.[81–83] Their irregular shapes and their spectroscopic characteristics are similar to those of D-type asteroids,[84,85] or Amalthea,[44] which are mostly located in the outer AB and in the outer Solar System. It was initially suggested as a possible origin by an atmospheric drag capture mechanism for these small satellites.[86,87] However, the orbits of Deimos and Phobos are nearly circular and coplanar to the orbit of Mars, and the capture scenario requires the removal of the atmosphere drag at ≈ 6 Mars radii once the capture process is complete; this is an improbable succession of events that make this process quite unlikely.[88]

Alternative scenarios proposed were through accretion disk formed by one or more giant impacts with impactors ≈0.01 × Mars' mass[89] or an oblique impact with a 10^{-3} Mars' mass-sized body.[10] Although it is theoretically possible to create both moons from an accretion disk of debris generated by these impacts, there are several problems that require a careful analysis.

First, the impact-generated accretion disk would have mixed debris (at least 35%[90]) coming from both impactor and target. Such an impact would have raised the temperature to 1,800–2,000 K driving any volatile (i.e., water) away from the disk leaving only dehydrated refractory elements.[10] This means that minerals like pyroxene and olivine should be visible in the spectrum of the formed moons, but this does not seem to be the case; no absorption features indicative of pyroxene and olivine were detected on both Deimos and Phobos.[84,91] It was pointed out since the Viking missions that even a bulk density of 2.0 ± 0.6 g cm^{-3} would have ruled out any basaltic composition.[92]

Second, Leone et al.[93] have demonstrated that it is not possible to create a Martian dichotomy with an oblique impact or with several basin-forming impacts; a vertical impact at the South Pole of Mars is absolutely necessary to produce enough energy to sustain internal heat and magnetic field and form the volcanic alignments observed on the surface of the planet.[94] If the putative true polar wander (TPW) may theoretically accommodate the current position of the putative Borealis basin with respect to the equatorial plane in which the moons formed,[95] it cannot accommodate the peculiar position of the loxodromic trajectories of the volcanic alignments ending up into the South Pole of Mars.

Third, once the moons formed from the accretion disk, tidal forces and libration would have pulled them back to the Martian surface. Phobos is currently losing altitude,[96] and only Deimos would have survived beyond synchronous rotation.[97] For this reason, moons formed from an earlier and primordial circum-Martian accretion disk (i.e., not formed by impact) would have had even less chance to survive.[80] At last, an additional hypothesis based on the splitting of a progenitor moon into two has been also suggested.[98,99]

The surface thermal properties of Deimos and Phobos have determined that both moons are covered with a uniform layer of finely divided material several cm thick.[100] However, the nature and composition of this surface layer are still unknown, and it might have a composition similar to that of D-type asteroids or be also characterized by Martian impact basin ejecta; that is why sample return missions are of valuable importance.[85,101–103] Thermal models for both Deimos and Phobos were developed since the late 80's to the early 90's,[104,105] based on Mariner[106–109] and Viking[81,100] data as the evolution of the standard thermal model (STM) of Mars developed by Kieffer et al.[110] The thermal model developed by Kührt and Giese[104] approximated the figure of Deimos and Phobos to triaxial ellipsoids[111] covered by regoliths and with no inner heat sources. The temperature T as a function of time t and depth x was expressed as

$$\rho c(T)\frac{\partial T}{\partial t} = \frac{\partial}{\partial x}\left[K(x,T)\frac{\partial T}{\partial t}\right] \quad \text{(Equation 2)}$$

where ρ is the density of the regolith (assumed 1 g cm^{-3}), c(T) the specific heat of the regolith expressed by[112]

$$c(T) = -34T^{1/2} + 8T - 0.2T^{3/2}, \quad \text{(Equation 3)}$$

and K (x, T) is the heat conduction coefficient of the regolith without gas pores written as the sum of the conductive term and the radiative term[113]:

$$K(T) = k_c(x) + k_r(T) \quad \text{(Equation 4)}$$

where k_c and k_r depend on the particle size of the regolith. Approximating Deimos and Phobos regolith to the lunar regolith and scaling for gravity, $k_c = 6 \times 10^{-4}$ $(x/m)^{3/5}$ W/K · m; K and c were taken at T = 200 K, and x = 0.[104] The results of the model can be effectively resumed in the following points: a) longitude dependence of the surface temperature which increases with increasing latitudes; b) no temperature differences along the equator at the same local times but differences up to 70 K along high latitudes; c) considerable temperature variations at the surfaces of Phobos and Deimos due to the low thermal conductivity of their regoliths and the absence of an atmosphere; and d) strong thermal stresses producing a superficial layer of a few centimeters consisting of very fine material, if the regolith grains are composed of various minerals with different thermal expansion coefficients.

Miranda

Miranda is the innermost and the smallest of the major satellites of Uranus; it has a radius of 235.8 ± 0.7 km and a density of 1.15 ± 0.15 g cm^{-3} indicative of a rock mass fraction between 0.2 and 0.4. The study of a spectrum between 1.2 and 2.5 μm revealed strong features indicative of water ice and a weak feature near 2.33 μm indicative of CH-bearing species or hydroxylated silicate (i.e., serpentine).[7] Serpentine is the altered product of olivine in aqueous environment,[114,115] and olivine is notoriously a component of basaltic magma. Miranda, like other Uranian moons, is dominated by a mixture of H_2O ice and an isotropically scattering dark material interpreted as carbonaceous in origin.[116,117]

Unfortunately, available data do not give sufficient certainty and we can only speculate that the dark material might be a component of basaltic composition in the subsurface of Miranda.

Miranda is thought to host a subsurface ocean, but it would freeze in a few hundred million years in absence of a long-term heat source.[15] According to the model by Szulágyi et al.,[14] Miranda formed like the other Uranus' moons in a circumuranian disk not generated by impacts in the first couple of 10^5 years. In this case, Miranda may have been formed sufficiently early to contain short-lived radiogenic elements like ^{26}Al; however, the moon may have also been subject to tidal heating after the ^{26}Al heat source exhausted.[15] Miranda is similar in size to the Saturnian moons Mimas and Enceladus, and its surface is divided in geologically old areas, around 3.9–4.3 Ga, and the younger (Elsinore, Arden, and Inverness) coronae areas between 0.1 and 1.2 Ga.[118] This interpretation would suggest that Miranda has been geologically active for quite long time after its formation thus implying that some mechanism of internal heat has been active for long time as well or that the uncertainty in crater count ages might be much higher than expected. In the former case, long-lived radiogenic heating must have been somehow involved given that any ongoing tidal heating process would still be keeping the moon active as well as in the case of Enceladus. In the latter case, the residual heating from its original formation may have contributed to the geological activity until the end long time ago.

The density difference with Enceladus, 1.15 g cm^{-3} vs. 1.61 g cm^{-3}, and the density similarity with Mimas, 1.15 g cm^{-3} vs. 1.149 g cm^{-3}, suggest a compositional similarity with Mimas and a compositional difference with Enceladus. A higher rock fraction increases the possibility of a higher abundance of long-lived radiogenic elements that still keep Enceladus warm inside, although such an abundance is regarded as an exception in such a small satellite.[23] That is why Enceladus is still active while Mimas and Miranda are not, despite their closeness to their respective planets that should favor tidal heating instead.

IGNEOUS PROCESSES IN DWARF PLANETS

Dwarf planets are mostly found in the outer Solar System; the only exception is Ceres that is located in the AB, which is the border between the inner and outer Solar System. Although the inner Solar System is characterized by bodies with a higher average density and thus a much higher rocky fraction than the bodies of the outer Solar System, the bulk density of Ceres (2.162 g cm^{-3}) is not dramatically different from that of Pluto (1.854 g cm^{-3}), Haumea (1.885 g cm^{-3}), or Sedna (2.000 g cm^{-3}). This means that the rocky fraction they contain was more or less uniformly available in the original protoplanetary disk that formed the Solar System.

Ceres

Ceres is the largest body in the AB with its 476.2 $\pm$ 1.7 km radius, and pre-Dawn observations interpreted it as a differentiated body in hydrostatic equilibrium of average bulk density 2,077 $\pm$ 36 kg m^{-3}.[119] The National Aeronautics and Space Administration (NASA) Dawn mission allowed more accurate measurements revealing an average bulk density of 2,162 $\pm$ 8 kg m^{-3}.[120] The average bulk density of Ceres permits a range of compositions for both crust and mantle, including a dense core,[121] that has been translated into a two-layers model consisting of a 41.0 km crust with 1,287 kg m^{-3} density overlying a mantle of 428.8 km radius with 2,434 kg m^{-3} density.[122] Another two-layers model assumed a core density of 2,460–2,900 kg m^{-3} and an outer shell of 70–190 km with density of 1,680–1,950 kg m^{-3}.[120] Additional improvements included a dense core in a three-layers model in which the following ranges were evaluated: crust (1,150–1,450 kg m^{-3}), mantle (1,650–2,450 kg m^{-3}), and core (1,950–5,150 kg m^{-3}); as a result, an average bulk density of 2,367 $\pm$ 26 kg m^{-3} was found.[121]

Pre-Dawn observations suggested that the interpreted presence of brucite and carbonate assemblages may be the product of altered olivine-rich materials on Ceres.[123] Post-Dawn data confirmed the presence of serpentine and carbonates on the surface of Ceres but did not confirm brucite.[6] The presence of NH_4-phyllosilicates, such as serpentine and smectites,[124] is particularly strong in craters Dantu, Darzamat, Ikapati, Inamahari, Kerwan, Kumitoga, Toharu, and Urvara, whereas it is in lower concentrations in craters Fejokoo, Haulani, Jarimba, Kirnis, Occator, Rongo, and Yalode; such a variability in concentration observed in craters of different sizes and ages suggests that it may be due to endogenous processes and thus not related to contamination of impactors.[125] Some of these craters are also floor-fractured craters (FFC), such as Dantu, Ikapati, Occator, and Yalode,[126] with the addition of Azacca.[127]

At the beginning, two processes were proposed to explain the formation of the FFC observed in the various bodies of the inner Solar System: topographic viscous relaxation[128] and magmatic intrusion.[129] During the years the process of magmatic intrusion gained more consensus[94,130–137] in explaining the FFC also because viscous relaxation is not a viable mechanism for craters with diameters <60 km.[138] In the specific case of Ceres, cryomagmatism was invoked to explain the morphology of the FFC Occator.[19] However, cryomagmatism cannot explain the concurrent presence of dark materials and serpentine observed on the floors of the FFC on Ceres. The possibility that serpentine may come from the aqueous alteration of olivine,[114,115,139] which is a component of basaltic lava, cannot be excluded. Actually, if Ceres followed a similar path to that of carbonaceous chondrite (CC), aqueous alteration of mafic, or even ultramafic material, may have occurred quite rapidly (4–5 Ma after CAI) consistently with the decay of short-lived radiogenic elements like ^{26}Al as possible heat source.[18]

According to the thermal model of Neveu and Desch,[140] based on the decay of both long-lived (^{4} K, ^{232}Th, ^{235}U, and ^{238}U) and short-lived (^{26}Al) radionuclides present in the rock at Ivuna-type CI abundances, the temperature inside Ceres raised to 600 K in the core and to 300 K at the core-mantle boundary (CMB). As a result of this thermal model, differentiation may have occurred 1 Ma after accretion (which may have occurred 1 or 7 Ma after CAI) forming a rocky core of 363 km in radius overlain by a 112 km-thick muddy hydrosphere vigorously convecting for about 60 Ma.[140]

Other thermal models[141,142] obtained essentially similar results. This could be a suitable environment for cryovolcanic processes with aqueous alteration of olivine contained in the rocky core. The white cryovolcanic plains of Enceladus, for example, do not show the same dark materials mantling the FFC observed on Ceres. Cryovolcanism might easily explain the geomorphology found at Ahuna Mons,[37] but

it leaves more than a doubt in explaining the geomorphology of FFCs on Ceres strikingly similar to those formed by basaltic lava and found in lunar, Martian, and Venusian surfaces. Available Dawn data show that these dark materials are more in line with CC composition,[18,124,143,144] which has olivine and pyroxene among its primary phases.[18] Therefore, if the dark materials observed in the FFCs are the product of earlier igneous processes similar to those occurred in other small bodies of the Solar System (e.g., 4 Vesta), Ceres might be the only body of the Solar System which hosted both hot and cold volcanism, maybe in different periods or stages of evolution, cryovolcanism being relatively younger with respect to hot volcanism.[145]

Haumea

Lacking spacecraft data yet, the information that we have about Haumea comes from telescope observational data and computer modeling. Although it is known that Haumea is on average 50.593 au distant from the Sun and holds a ring and two satellites (Hi'iaka and Namaka), there is still uncertainty on its basic parameters like average size between ≈720 km[146] and ≈795 km[147] of mean radius, and density between 1,885 kg m^{-3} and 2, 495 kg m^{-3} depending on the triaxial ellipsoid used in the calculations.[147,148] A robust analysis of these results has shown that Haumea's core might have a density between 2,600 kg m^{-3} and 2,740 kg m^{-3}, thus suggesting aqueous alteration of the olivine with serpentinization of the core by comparison with the similar density of phyllosilicates such as montmorillonite, kaolinite, illite, and mica through the reaction

$$1.000\ (Mg_{0.71}Fe_{0.29})_2\ SiO_4 + 1.142\ H_2O \rightarrow 0.474\ Mg_3Si_2O_5(OH)_4 + 0.193 Fe_3O_4 + 0.052\ SiO_2 + 0.194 H_2 \quad \text{(Equation 5)}$$

Before the reaction the total density of olivine (3,589 kg m^{-3}) interacting with water ice (921 kg m^{-3}) is 2,697 kg m^{-3}, and after the reaction it is 2,874 kg m^{-3}; allowing 10% of porosity that is typical of CC, the total density of the altered olivine would be 2,612 kg m^{-3} and thus very similar to the density of Haumea's core inferred through the calculations.[148] Obviously, this is entirely theoretical and ground truth is necessary to verify whether the products of the reaction are really present on the surface of Haumea. Available spectroscopic observations have put constraints on the possible upper limits of serpentine, kaolinite, orthopyroxene, and olivine in the measure of 7%, 4%, 7%, and 5%, respectively.[11]

Not much is known about the formation and thermal history of Haumea. A massive collision may have stripped off much of its icy mantle and gave it its fast rotation period of about 4 h. A few near-infrared (IR) spectra match laboratory spectra of crystalline ice[149] possibly suggesting formation by cryovolcanic processes. Relatively large bodies like Haumea are thought to be characterized by impact cratering and not by disruptive collisions; however Haumea is thought to be the parent body of the only collisional family of Transneptunian Object (TNO)s identified so far.[150–152] Brown et al.[153] suggested that the four most water-rich Kuiper Belt Objects (KBOs) and Hi'iaka are basically made of the fragments ejected by such a massive collision. A "graze and merge" impact between two equal bodies of 650 km in diameter colliding at 0.9 km s^{-1} was used to explain the formation of Haumea and its family.[154] Thirty-five TNOs belonging to this collisional family were identified so far[155]; among these, its moons Hi'iaka, ~383 km in diameter, and Namaka, ~193 km in diameter, with Salacia and Makemake, are included as dynamical interlopers and thus excluded as possible members of the collisional family having comparable size to Haumea.[152,156]

120347 Salacia-42355 Actaea binary system

Formerly denominated as KBO 2004 SB60,[149] its thermal evolution is poorly known. Classified as a classical KBO, 120347 Salacia has an average diameter of 905 ± 80 km and forms a binary system with its satellite 303 ± 27 km of diameter named 42355 Actaea.[157] The 120347 Salacia system is located at a distance of ~ 42.3 au from the Sun, in a region of orbital elements associated to the collisional family of Haumea (41.6 < a <43.6 au[156]), and it is quite different from the other members of the family for its lack of strong water-ice near-IR absorption features,[157] low albedo, and flat spectrum consistent with 90% ± 20% of amorphous silicates and 10% ± 20% of H_2O ice.[158] Other measurements report even less than 5% of water ice, but its low albedo is comparable to that of many other small KBOs.[149] However, its (binary system) density of 1,160 kg m^{-3} is quite low for a body of this composition; the lack of information on the state of the few ices available does not allow to understand whether it underwent cryovolcanic processes or not.

The low density of the system suggests that it must be significantly porous, and, because of these physical characteristics, Stansberry et al.[157] concluded that it is unlikely that 120347 Salacia belongs to the Haumea collisional family. Malamud and Prialnik[16] obtained a higher density of 1,350 kg m^{-3} on the basis of a radius of 420.8 km for 120347 Salacia, which is quite close to the density of 1,370 kg m^{-3} obtained by Grundy et al.[159] Available modeling of the internal structure of 120347 Salacia shows a 125 km-thick (in radius) ice-rich mantle between ~1,400 and ~1,100 kg m^{-3} of density overlying a denser (~2,100–1,800 kg m^{-3}) and serpentinized 250 km-thick (in radius) rocky core; between these two layers there is a 25 km-thick layer of transition in which a density drop from 1,800 to 917 kg m^{-3} is observable. The last 20 km to the surface are characterized by amorphous ice with a gradual transition to a 5 km layer in which crystalline ice occurs.[16] Worth noting that Malamud and Prialnik[16] assumed a long-term radioactive heating in their modeling with a peak temperature reaching in 1.8 Ga after CAI and a still warm temperature, around 300 K, in current days. If the modeling is correct, this means that 120347 Salacia might still have an internal liquid water layer.

Orcus

Orcus is a dwarf planet with a diameter of 946 ± 73 km located at an average distance of 47.90 au from the Sun,[160] being in 3:2 resonance with Neptune like Pluto and thus belonging to the Plutino class,[161] and holds a small satellite of ~300 km diameter named Vanth.[162] Based on

albedo estimates, large uncertainties existed between 900 km and 280 km or 860 km and 380 km for Orcus and Vanth, respectively.[162] However, the diameter of Orcus was subsequently refined to 850 ± 90 km[163,164] whereas the diameter of Vanth was refined to 443 ± 10 km thanks to a stellar occultation.[165] The mass of the Orcus-Vanth system was calculated by Brown et al.[162] as 6.32 ± 0.05 × 10^{23} g whereas the derived system density was 1,600 kg m^{-3} on the assumption of similar albedo for the two bodies. Other authors derived a different density of 1,530 kg m^{-3} on the basis of high albedo for Orcus and low albedo for Vanth.[16,166] Although the sizes of Orcus and Salacia are almost similar, their densities are quite different thus implying a higher rocky fraction in the core and/or a thinner mantle within Orcus.

Available modeling by Malamud and Prialnik[16] assumed both higher rocky fraction with a density ranging from 2,700 to 1,700 kg m^{-3} in a ~350 km-thick (in radius) Orcus' core and a ~10 km-thick outer layer, where amorphous ice survives, thus leaving only ~110 km in radius for the water ice-rich mantle. Also, the thermal evolution of Orcus shows some differences with Salacia; although the general trend is similar, a higher peak temperature of 900 K was reached 400 Ma after Salacia and still keeping warm at an amazing (for the outer Solar System) temperature of 550 K until current days.[16] If the modeling is correct, ongoing cryovolcanic activity should be expected and possibly detected on Orcus. The detection of crystalline ice, along with methane and ammonia ice, on the surface of Orcus[161,164,167] is consistent with possible cryovolcanic processes, ongoing[22] or past at least, crystalline ice being able to survive irradiation doses up to 160 ± 30 eV for T ≥ 30 K.[167]

Quaoar

Quaoar-Weywot is another binary system located at 43.574 au from the Sun,[168] in which Weywot is the satellite, with respective diameters of ~1,150 km and 90 km; these numbers constitute an average among various measurements that span from ~890 to ~1,300 km for Quaoar.[17,169–171] The initially proposed density for Quaoar, 4,200 ± 1,300 kg m^{-3}, is probably the highest among the KBOs thus suggesting a thin veneer of various ices (water, methane, ethane) on the surface of an essentially rocky body.[169,172] However, subsequent stellar occultation data showed a density of 1,990 ± 460 kg m^{-3} [170] thus suggesting a more ice-rich component.[173] The possible presence of crystalline ice on the surface proposed by Jewitt and Luu[17] opened the possibility of cryovolcanism on Quaoar because crystalline ice is converted into amorphous ice in 1.5 Ma under the flux of galactic cosmic rays (GCRs).[8,22] Available thermal modeling based on both short- and long-lived radiogenic elements, assuming a homogeneous distribution in the protoplanetary disk and a density of the rocky material not less than 3,600 kg m^{-3}, suggested a steady core temperature of 500 K in the 0.45 and 45 Ma formation time scenarios whereas a temperature of 650 K is reached in the 4.5 Ma formation time scenario.[22]

Sedna

Sedna, with its perihelion distance of 76 au and aphelion distance of 921 au, is the most distant dwarf planet observed and has a diameter of about 1,300 km.[174] Its mass was not determined yet, and thus its density could not be determined either. It was classified as an extended scattered disk object, or a detached object, according to the classification of Gladman et al.[175] Not much is known about Sedna due to its distance from the Sun that poses it at the limit of observability. Due to its relatively small size and low internal heat, Sedna might be subject to serpentinization processes (see Equation 5) with liquid water percolating through a possible microfracturing system, possibly extending down to 97 km of depth, and entering in contact with unaltered rocks containing iron-bearing olivine and pyroxene.[12] Among the products of this reaction, H_2 is released in the surrounding environment. Although Sedna is believed to be differentiated and hosting a subsurface ocean,[176,177] spectroscopic observations reported the detection of methane and nitrogen on its surface.[178] Subsequent spectra in the visible and near-IR obtained through the European Southern Observatory - Very Large Telescope (ESO-VLT) telescope could be modeled with tholin, serpentine, and water ice; one of the past spectra obtained during the observations made in October 2005 could be best modeled with methanol instead of methane and the addition of serpentine and olivine.[174] Cruikshank[179] noticed that at least four spectrally active components, plus spectrally neutral grains of amorphous carbon, are needed to accommodate spectral models with available spectral data: tholin, water ice, methanol ice, and olivine. These components were also found on typical cometary nuclei and on the centaur 5145 Pholus.[180]

DISCUSSION

Based on the results of the previous work on asteroids and comets (Leone and Tanaka[1]), the eventual presence of olivine in the small satellites and dwarf planets of the Solar System does not necessarily mean that it is the result of volcanism as we have already seen that it could be recycled from previous nebular processes. However, the presence of serpentine, which is the product of alteration of olivine in aqueous environment, must be studied with more attention because it could also be the sign of a possible hydrothermal environment typical of volcanic processes. The overview of the inferred or modeled temperatures during the formation and evolution of the small bodies of the Solar System is based on the assumption that impacts and radiogenic heat sources were at the basis of the igneous processes. It must be seen whether these igneous processes developed in some form of volcanism, either hot or cold, which could have contributed to the formation of the serpentine. If further confirmed by future detections, the presence of olivine and its altered form serpentine is quite ubiquitous even in the outer Solar System and beyond. As already seen in asteroids and comets,[1] the origin of olivine is likely nebular. That is, it was already present in the dusty component of the protoplanetary nebula from which the Solar System formed, and it was probably recycled many times from the origin of our galaxy in the universe. The presence of olivine in the interstellar dust also means that it is likely present in the interstellar space from which it was entrained in the long-period comets. Due to its high melting point, 2,163 ± 25 K,[181] olivine is the first mineral that crystallizes in volcanic processes and thus it is often found in its crystalline form. However, if its melting temperature can be overcome by heating processes, it goes back into the volcanic (or protoplanetary) melts. The melting temperature of the olivine was reached during the

southern polar giant impact (SPGI) on Mars,[93] for example, and could be reached close to any star similar to our Sun or under the heating action of radiogenic elements. However, crystalline olivine can also be formed by thermal annealing on amorphous ferromagnesian silicate under vacuum at temperatures of 870–1,020 K.[182]

Although igneous processes were quite common at the beginning of the Solar System,[1] not all the satellites and dwarf planets developed evident volcanism or cryovolcanism. Mimas, which is debated whether geologically active or not (Rhoden et al.[183] and references therein) despite levels of tidal dissipation 30 times higher than those within Enceladus,[184] and Makemake, which is not included in the list of potential candidates for former cryovolcanism, are examples.[185] Yet, the evidence of past cryovolcanism on the surfaces of small satellites and dwarf planets is quite common in the outer Solar System. With the exception of Amalthea that does not show evident signs of either volcanism or cryovolcanism and that probably finished its internal heat 7.05×10^5 years $\pm$ 3.4% after CAI, an estimate based on the half-life of ^{26}Al,[58] a long-lived radiogenic heating source must have been certainly involved in the other bodies (i.e., Miranda) included in this review. Regardless of initial formation mechanisms, whether by impact or not, the initial internal heat (and thus either volcanism or cryovolcanism) would not last long without a long-lived radiogenic or tidal source. Aside from Io and Enceladus, (possibly Europa) still active today; possibly Miranda, active in the past; and Mimas, with a potential subsurface ocean,[183] no tidal heating is involved in the other bodies. Therefore, the obvious conclusion is that the other bodies must have had some long-lived radiogenic source or terminated their activity long time ago when the residual heating of formation was over. The relatively fresh, not intensely cratered, surfaces of Ceres and Pluto lead toward the long-lived radiogenic source, but a word of caution must be spent on the ages estimated through crater counts because on Mars they were quite fallacious or showed very high uncertainties at least.[135,186] This means that the past activities of Ceres and Pluto might not necessarily be so recent; the cleaning process of the orbits producing the majority of the impacts occurred in the first few millions of years after planetary formation,[187,188] which corresponds to the Pre-Noachian on Mars.[186] It is now clear that quantifying the age of the geological activity on these "fresh" surfaces needs accurate assumptions about the initial content of long-lived radiogenic elements in their corresponding bodies.

CONCLUSIONS

From the analysis of the igneous processes observed in the satellites and the dwarf planets of the Solar System, we draw the following conclusions.

(1) The dichotomy volcanism-cryovolcanism, being its border located within the AB and just before the beginning of the snow line, also marks the border between inner and outer Solar System like the AB does. There are exceptions to this statement: 1) the possible existence of both volcanism and cryovolcanism on Ceres, although it may be regarded as the exact border, and 2) the volcanism of Io (being located outside the border) so different from the cryovolcanism of Europa, where the difference in the total amount of tidal dissipation makes the difference in the type of volcanism.
(2) The presence of long-lived radiogenic sources is an essential requirement to maintain active geological activity of a body of the Solar System.
(3) The situation of the most distant dwarf planets, those located beyond the orbit of Pluto, is still unknown, and we are not certain yet if others will be discovered in future. From those included in this review, it is possible to understand that some hydrothermal process must be invoked in order to justify the assumption of serpentine in the modeling of the internal structure. Being some dwarf planets believed to be ocean worlds (i.e., Pluto, Sedna), the obvious conclusion is that some liquid water could be available at depth and could be the basis for hydrothermal environments provided some radiogenic heat is still available.
(4) The process of conversion of amorphous ice into crystalline ice opens the possibility of cryovolcanism on the dwarf planets but not the final evidence for it because we have not yet any idea of how fast or slow this process occurred.

A pending question in this work, but left to future work, is the cause(s) of both short-lived and long-lived distribution of radiogenic elements within the Solar System. After the discovery of ^{26}Al in CAIs of primitive meteorites, its origin also remains an open question. It is generally thought that ^{26}Al atoms are produced and injected in presolar nebulas by massive (e.g., Wolf-Rayet) stars and/or by Type II supernovae, which may also have triggered the formation of the Solar System.

LIMITATIONS OF THE STUDY

Aside from Ceres, which was studied through spacecraft data, the spectroscopic information about the most distant dwarf planets (excluding Pluto and its moon Charon) is still subject to various interpretations and thus may provide some uncertainty.

ACKNOWLEDGMENTS

The authors are grateful to Daniele Gasparri for the figure, to Claudio Pereira Pinto for the graphical abstract, and to an anonymous reviewer who helped to improve the manuscript.

AUTHOR CONTRIBUTIONS

G.L. and H.T. conceived and designed the study and drafted and reviewed the manuscript. Both authors read and approved the manuscript.

DECLARATION OF INTERESTS

The authors declare no competing interests.

REFERENCES

1. Leone, G., and Tanaka, H.K.M. (2023). Igneous processes in the small bodies of the Solar System I. Asteroids and Comets. iScience *26*, 107160. https://doi.org/10.1016/j.isci.2023.107160.
2. Cameron, A.G.W., and Pollack, J.B. (1976). In On the origin of the solar system and of Jupiter and its satellites, Jupiter and T. Gehrels, eds. (University of Arizona Press), pp. 61–84.
3. Wong, M.H., de Pater, I., Showalter, M.R., Roe, H.G., Macintosh, B., and Verbanac, G. (2006). Ground-based near infrared spectroscopy of Jupiter's ring and moons. Icarus *185*, 403–415. https://doi.org/10.1016/J.ICARUS.2006.07.007.
4. Throop, H., West, R.A., Burns, J.A., Showalter, M.R., Nicholson, P.D., and Porco, C.C. (2004). The jovian rings: new results derived from Cassini, Galileo, Voyager, and Earth-based observations. Icarus *172*, 59–77. https://doi.org/10.1016/J.ICARUS.2003.12.020.
5. Takato, N., Bus, S.J., Terada, H., Pyo, T.S., and Kobayashi, N. (2004). Detection of a deep 3-μm absorption feature in the spectrum of Amalthea (JV). Science *306*, 2224–2227. https://doi.org/10.1126/SCIENCE.1105427/SUPPL_FILE/TAKATO_SOM.PDF.
6. Castillo-Rogez, J., Neveu, M., McSween, H.Y., Fu, R.R., Toplis, M.J., and Prettyman, T. (2018). Insights into Ceres's evolution from surface composition. Meteorit. Planet. Sci. *53*, 1820–1843. https://doi.org/10.1111/MAPS.13181.
7. Bauer, J., Roush, T.L., Geballe, T.R., Meech, K.J., Owen, T.C., Vacca, W.D., Rayner, J.T., and Jim, K.T.C. (2002). The Near Infrared Spectrum of Miranda: Evidence of Crystalline Water Ice. Icarus *158*, 178–190. https://doi.org/10.1006/ICAR.2002.6876.
8. Cook, J.C., Desch, S.J., Roush, T.L., Trujillo, C.A., and Geballe, T.R. (2007). Near Infrared Spectroscopy of Charon: Possible Evidence for Cryovolcanism on Kuiper Belt Objects. Astrophys. J. *663*, 1406–1419. https://doi.org/10.1086/518222/FULLTEXT/.
9. Holm, N.G., Oze, C., Mousis, O., Waite, J.H., and Guilbert-Lepoutre, A. (2015). Serpentinization and the Formation of H2 and CH4 on Celestial Bodies (Planets, Moons, Comets). Astrobiology *15*, 587–600. https://doi.org/10.1089/AST.2014.1188/ASSET/IMAGES/LARGE/FIGURE5.JPEG.
10. Canup, R., and Salmon, J. (2018). Origin of Phobos and Deimos by the impact of a Vesta-to-Ceres sized body with Mars. Sci. Adv. *4*, eaar6887. https://doi.org/10.1126/SCIADV.AAR6887/SUPPL_FILE/AAR6887_SM.PDF.
11. Pinilla-Alonso, N., Brunetto, R., Licandro, J., Gil-Hutton, R., Roush, T.L., and Strazzulla, G. (2009). The surface of (136108) Haumea (2003 EL61), the largest carbon-depleted object in the trans-Neptunian belt. Astron. Astrophys. *496*, 547–556. https://doi.org/10.1051/0004-6361/200809733.
12. Vance, S.D., and Melwani Daswani, M. (2020). Serpentinite and the search for life beyond Earth. Philos. Trans. R. Soc. A *378*, 20180421. https://doi.org/10.1098/RSTA.2018.0421.
13. Desch, S.J., and Neveu, M. (2017). Differentiation and cryovolcanism on Charon: A view before and after New Horizons. Icarus *287*, 175–186. https://doi.org/10.1016/J.ICARUS.2016.11.037.
14. Szulágyi, J., Cilibrasi, M., and Mayer, L. (2018). In Situ Formation of Icy Moons of Uranus and Neptune. Astrophys. J. Lett. *868*, L13. https://doi.org/10.3847/2041-8213/AAEED6.
15. Weiss, B.P., Biersteker, J.B., Colicci, V., Goode, A., Castillo-Rogez, J.C., Petropoulos, A.E., and Balint, T.S. (2021). Searching for Subsurface Oceans on the Moons of Uranus Using Magnetic Induction. Geophys. Res. Lett. *48*, e2021GL094758. https://doi.org/10.1029/2021GL094758.
16. Malamud, U., and Prialnik, D. (2015). Modeling Kuiper belt objects Charon, Orcus and Salacia by means of a new equation of state for porous icy bodies. Icarus *246*, 21–36. https://doi.org/10.1016/J.ICARUS.2014.02.027.
17. Jewitt, D.C., and Luu, J. (2004). Crystalline water ice on the Kuiper belt object (50000) Quaoar. Nat *432*, 731–733. https://doi.org/10.1038/nature03111.
18. McSween, H.Y., Emery, J.P., Rivkin, A.S., Toplis, M.J., C. Castillo-Rogez, J., Prettyman, T.H., De Sanctis, M.C., Pieters, C.M., Raymond, C.A., and Russell, C.T. (2018). Carbonaceous chondrites as analogs for the composition and alteration of Ceres. Meteorit. Planet. Sci. *53*, 1793–1804. https://doi.org/10.1111/MAPS.12947.
19. Buczkowski, D.L., Williams, D.A., Scully, J.E.C., Mest, S.C., Crown, D.A., Schenk, P.M., Jaumann, R., Roatsch, T., Preusker, F., Nathues, A., et al. (2018). The geology of the occator quadrangle of dwarf planet Ceres: Floor-fractured craters and other geomorphic evidence of cryomagmatism. Icarus *316*, 128–139. https://doi.org/10.1016/J.ICARUS.2017.05.025.
20. Martin, C.R., and Binzel, R.P. (2021). Ammonia-water freezing as a mechanism for recent cryovolcanism on Pluto. Icarus *356*, 113763. https://doi.org/10.1016/J.ICARUS.2020.113763.
21. Sparks, W.B., Schmidt, B.E., McGrath, M.A., Hand, K.P., Spencer, J.R., Cracraft, M., and Deustua, S.E. (2017). Active Cryovolcanism on Europa? Astrophys. J. Lett. *839*, L18. https://doi.org/10.3847/2041-8213/AA67F8.
22. Shchuko, O.B., Shchuko, S.D., Kartashov, D.V., and Orosei, R. (2014). Conditions for liquid or icy core existence in KBO objects: Numerical simulations for Orcus and Quaoar. Planet. Space Sci. *104*, 147–155. https://doi.org/10.1016/J.PSS.2014.01.022.
23. Leone, G., Bieger, K., and Soto, M. (2021). Identification of Possible Heat Sources for the Thermal Output of Enceladus. Planet. Sci. J. *2*, 29. https://doi.org/10.3847/PSJ/abdb33.
24. Geissler, P. (2015). Cryovolcanism in the Outer Solar System. Encycl. Volcanoes, 763–776. https://doi.org/10.1016/B978-0-12-385938-9.00044-4.
25. Helfenstein, P., and Porco, C.C. (2015). ENCELADUS' GEYSERS: RELATION TO GEOLOGICAL FEATURES. Astron. J. *150*, 96. https://doi.org/10.1088/0004-6256/150/3/96.
26. Crawford, G.D., and Stevenson, D.J. (1988). Gas-driven water volcanism and the resurfacing of Europa. Icarus *73*, 66–79. https://doi.org/10.1016/0019-1035(88)90085-1.
27. Wilson, L., Head, J.W., and Pappalardo, R.T. (1997). Eruption of lava flows on Europa: Theory and application to Thrace Macula. J. Geophys. Res. *102*, 9263–9272. https://doi.org/10.1029/97JE00412.
28. Showman, A.P., Mosqueira, I., and Head, J.W. (2004). On the resurfacing of Ganymede by liquid–water volcanism. Icarus *172*, 625–640. https://doi.org/10.1016/J.ICARUS.2004.07.011.
29. Nimmo, F., Spencer, J.R., Pappalardo, R.T., and Mullen, M.E. (2007). Shear heating as the origin of the plumes and heat flux on Enceladus. Nature *447*, 289–291. https://doi.org/10.1038/nature05783.
30. Smith-Konter, B., and Pappalardo, R.T. (2008). Tidally driven stress accumulation and shear failure of Enceladus's tiger stripes. Icarus *198*, 435–451. https://doi.org/10.1016/j.icarus.2008.07.005.
31. Wilson, L., and Keil, K. (1996). Volcanic eruptions and intrusions on the asteroid 4 Vesta. J. Geophys. Res. *101*, 18927–18940. https://doi.org/10.1029/96JE01390.
32. Williams, D.A., O'Brien, D.P., Schenk, P.M., Denevi, B.W., Carsenty, U., Marchi, S., Scully, J.E., Jaumann, R., De Sanctis, M.C., Palomba, E., et al. (2014). Lobate and flow-like features on asteroid Vesta. Planet. Space Sci. *103*, 24–35. https://doi.org/10.1016/j.pss.2013.06.017.
33. Palomba, E., Longobardo, A., De Sanctis, M.C., Zinzi, A., Ammannito, E., Marchi, S., Tosi, F., Zambon, F., Capria, M.T., Russell, C.T., et al. (2015). Detection of new olivine-rich locations on Vesta. Icarus *258*, 120–134. https://doi.org/10.1016/J.ICARUS.2015.06.011.
34. Smith, B.A., Soderblom, L.A., Beebe, R., Boyce, J., Briggs, G., Carr, M., Collins, S.A., Cook, A.F., Danielson, G.E., Davies, M.E., et al. (1979). The Galilean Satellites and Jupiter: Voyager 2 Imaging Science Results. Science *206*, 927–950. https://doi.org/10.1126/SCIENCE.206.4421.927.
35. Shalygin, E.V., Markiewicz, W.J., Basilevsky, A.T., Titov, D.V., Ignatiev, N.I., and Head, J.W. (2015). Active volcanism on Venus in the Ganiki Chasma rift zone. Geophys. Res. Lett. *42*, 4762–4769. https://doi.org/10.1002/2015GL064088.
36. D'Incecco, P., Filiberto, J., López, I., Gorinov, D.A., and Komatsu, G. (2021). Idunn Mons: Evidence for Ongoing Volcano-tectonic Activity and Atmospheric Implications on Venus. Planet. Sci. J. *2*, 215. https://doi.org/10.3847/PSJ/AC2258.
37. Ruesch, O., Platz, T., Schenk, P., McFadden, L.A., Castillo-Rogez, J.C., Quick, L.C., Byrne, S., Preusker, F., O'Brien, D.P., Schmedemann, N., et al. (2016). Cryovolcanism on Ceres. Science *353*, 353.

https://doi.org/10.1126/SCIENCE.AAF4286/ASSET/2CF22288-6587-48A7-8583-2322EDF9449E/ASSETS/GRAPHIC/353_AAF4286_FA.JPEG.
38. Spencer, J.R., Pearl, J.C., Segura, M., Flasar, F.M., Mamoutkine, A., Romani, P., Buratti, B.J., Hendrix, A.R., Spilker, L.J., and Lopes, R.M.C. (2006). Cassini encounters Enceladus: Background and the discovery of a south polar hot spot. Science *311*, 1401–1405. https://doi.org/10.1126/science.1121661.
39. Peale, S.J., Cassen, P., and Reynolds, R.T. (1979). Melting of Io by Tidal Dissipation. Science *203*, 892–894. https://doi.org/10.1126/SCIENCE.203.4383.892.
40. Veeder, G.J., Davies, A.G., Matson, D.L., Johnson, T.V., Williams, D.A., and Radebaugh, J. (2012). Io: Volcanic thermal sources and global heat flow. Icarus *219*, 701–722. https://doi.org/10.1016/j.icarus.2012.04.004.
41. Ross, M.N., and Schubert, G. (1987). Tidal heating in an internal ocean model of Europa. Nat *325*, 133–134. https://doi.org/10.1038/325133a0.
42. Lecar, M., Podolak, M., Sasselov, D., and Chiang, E. (2006). On the Location of the Snow Line in a Protoplanetary Disk. Astrophys. J. *640*, 1115–1118. https://doi.org/10.1086/500287/FULLTEXT/.
43. Henin, B. (2018). The Frost Line. In Exploring the Ocean Worlds of Our Solar System (Springer), pp. 21–31. https://doi.org/10.1007/978-3-319-93476-1_2.
44. Gradie, J., Thomas, P., and Veverka, J. (1980). The surface composition of Amalthea. Icarus *44*, 373–387. https://doi.org/10.1016/0019-1035(80)90032-9.
45. Veverka, J., Thomas, P., Davies, M., and Morrison, D. (1981). Amalthea: Voyager imaging results. J. Geophys. Res. *86*, 8675–8682. https://doi.org/10.1029/JA086IA10P08675.
46. Stooke, P.J. (1994). The geology of Amalthea. Earth Moon Planets *64*, 187–197. https://doi.org/10.1007/BF00604489.
47. Pollack, J.B., Burns, J.A., and Tauber, M.E. (1979). Gas drag in primordial circumplanetary envelopes: A mechanism for satellite capture. Icarus *37*, 587–611. https://doi.org/10.1016/0019-1035(79)90016-2.
48. Cruikshank, D., Dalle Ore, C.M., Roush, T.L., Geballe, T.R., Bergh, C., Cash, M.D., and Hartmann, W.K. (2001). Constraints on the Composition of Trojan Asteroid 624 Hektor. Icarus *153*, 348–360. https://doi.org/10.1006/ICAR.2001.6703.
49. Anderson, J.D., Johnson, T.V., Schubert, G., Asmar, S., Jacobson, R.A., Johnston, D., Lau, E.L., Lewis, G., Moore, W.B., Taylor, A., et al. (2005). Amalthea's Density Is Less Than That of Water. Science *308*, 1291–1293. https://doi.org/10.1126/SCIENCE.1110422.
50. Ockert-Bell, M.E., Burns, J.A., Daubar, I.J., Thomas, P.C., Veverka, J., Belton, M.J.S., and Klaasen, K.P. (1999). The Structure of Jupiter's Ring System as Revealed by the Galileo Imaging Experiment. Icarus *138*, 188–213. https://doi.org/10.1006/ICAR.1998.6072.
51. Cooper, N., Murray, C., Porco, C., and Spitale, J. (2006). Cassini ISS astrometric observations of the inner jovian satellites, Amalthea and Thebe. Icarus *181*, 223–234. https://doi.org/10.1016/J.ICARUS.2005.11.007.
52. Borisov, N., and Krüger, H. (2020). Electrostatic lofting of dust grains from the surfaces of Thebe and Amalthea. Planet. Space Sci. *183*, 104556. https://doi.org/10.1016/J.PSS.2018.06.005.
53. Lunine, J.I., and Stevenson, D.J. (1982). Formation of the galilean satellites in a gaseous nebula. Icarus *52*, 14–39. https://doi.org/10.1016/0019-1035(82)90166-X.
54. Canup, R.M., and Ward, W.R. (2002). Formation of the Galilean Satellites: Conditions of Accretion. Astron. J. *124*, 3404–3423. https://doi.org/10.1086/344684/FULLTEXT/.
55. Greenberg, R. (2010). The icy Jovian satellites after the Galileo mission. Rep. Prog. Phys. *73*, 036801. https://doi.org/10.1088/0034-4885/73/3/036801.
56. Samonelli, D.P. (1983). Amalthea: Implications of the temperature observed by Voyager. Icarus *54*, 524–538. https://doi.org/10.1016/0019-1035(83)90244-0.
57. Chyba, C.F., Hand, K.P., and Thomas, P.J. (2021). Magnetic induction heating of planetary satellites: Analytical formulae and applications. Icarus *360*, 114360. https://doi.org/10.1016/J.ICARUS.2021.114360.
58. Norris, T.L., Gancarz, A.J., Rokop, D.J., and Thomas, K.W. (1983). Half-life of 26Al. J. Geophys. Res. *88*, B331–B333. https://doi.org/10.1029/JB088IS01P0B331.
59. Moore, J.M., and McKinnon, W.B. (2021). Geologically Diverse Pluto and Charon: Implications for the Dwarf Planets of the Kuiper Belt. Annu. Rev. Earth Planet. Sci. *49*, 173–200. https://doi.org/10.1146/ANNUREV-EARTH-071720-051448.
60. Bierson, C.J., Nimmo, F., and McKinnon, W.B. (2018). Implications of the observed Pluto–Charon density contrast. Icarus *309*, 207–219. https://doi.org/10.1016/J.ICARUS.2018.03.007.
61. Bierson, C.J., Nimmo, F., and Stern, S.A. (2020). Evidence for a hot start and early ocean formation on Pluto. Nat. Geosci. *13*, 468–472. https://doi.org/10.1038/s41561-020-0595-0.
62. Leone, G. (2014). A network of lava tubes as the origin of Labyrinthus Noctis and Valles Marineris on Mars. J. Volcanol. Geotherm. Res. *277*, 1–8. https://doi.org/10.1016/j.jvolgeores.2014.01.011.
63. Lopes, R.M.C., Mitchell, K.L., Stofan, E.R., Lunine, J.I., Lorenz, R., Paganelli, F., Kirk, R.L., Wood, C.A., Wall, S.D., Robshaw, L.E., et al. (2007). Cryovolcanic features on Titan's surface as revealed by the Cassini Titan Radar Mapper. Icarus *186*, 395–412. https://doi.org/10.1016/J.ICARUS.2006.09.006.
64. Rhoden, A.R., Skjetne, H.L., Henning, W.G., Hurford, T.A., Walsh, K.J., Stern, S.A., Olkin, C.B., Spencer, J.R., Weaver, H.A., Young, L.A., and Ennico, K. (2020). Charon: A Brief History of Tides. JGR. Planets *125*, e2020JE006449. https://doi.org/10.1029/2020JE006449.
65. Brown, M.E., and Calvin, W.M. (2000). Evidence for Crystalline Water and Ammonia Ices on Pluto's Satellite Charon. Science *287*, 107–109. https://doi.org/10.1126/SCIENCE.287.5450.107.
66. Brown, M.E. (2002). Pluto and Charon: Formation, Seasons, Composition. Annu. Rev. Earth Planet Sci. *30*, 307–345. https://doi.org/10.1146/ANNUREV.EARTH.30.090401.095213.
67. Barr, A.C., and Collins, G.C. (2015). Tectonic activity on Pluto after the Charon-forming impact. Icarus *246*, 146–155. https://doi.org/10.1016/J.ICARUS.2014.03.042.
68. Malamud, U., Perets, H.B., and Schubert, G. (2017). The contraction/expansion history of Charon with implications for its planetary-scale tectonic belt. Mon. Not. R. Astron. Soc. *468*, 1056–1069. https://doi.org/10.1093/MNRAS/STX546.
69. Stern, S.A. (1992). THE PLUTO-CHARON SYSTEM. Annu. Rev. Astron. Astrophys. *30*, 185–233.
70. Canup, R.M. (2005). A giant impact origin of Pluto-Charon. Science *307*, 546–550. https://doi.org/10.1126/SCIENCE.1106818/SUPPL_FILE/CANUP.SOM.PDF.
71. Canup, R.M. (2012). Forming a moon with an Earth-like composition via a giant impact. Science *338*, 1052–1055. https://doi.org/10.1126/SCIENCE.1226073/SUPPL_FILE/CANUP.SM.PDF.
72. Sekine, Y., Genda, H., Kamata, S., and Funatsu, T. (2017). The Charon-forming giant impact as a source of Pluto's dark equatorial regions. Nat. Astron. 0031. https://doi.org/10.1038/s41550-016-0031.
73. Citron, R.I., Perets, H.B., and Aharonson, O. (2018). The Role of Multiple Giant Impacts in the Formation of the Earth–Moon System. Astrophys. J. *862*, 5. https://doi.org/10.3847/1538-4357/AACA2D.
74. Weaver, H.A., Stern, S.A., Mutchler, M.J., Steffl, A.J., Buie, M.W., Merline, W.J., Spencer, J.R., Young, E.F., and Young, L.A. (2006). Discovery of two new satellites of Pluto. Nat *439*, 943–945. https://doi.org/10.1038/nature04547.
75. Stern, S.A., Weaver, H.A., Steffl, A.J., Mutchler, M.J., Merline, W.J., Buie, M.W., Young, E.F., Young, L.A., and Spencer, J.R. (2006). A giant impact origin for Pluto's small moons and satellite multiplicity in the Kuiper belt. Nat *439*, 946–948. https://doi.org/10.1038/nature04548.
76. Ward, W.R., and Canup, R.M. (2006). Forced resonant migration of Pluto's outer satellites by charon. Science *313*, 1107–1109. https://doi.org/10.1126/SCIENCE.1127293/SUPPL_FILE/WARD_SOM.PDF.
77. Kenyon, S.J., and Bromley, B.C. (2013). THE FORMATION OF PLUTO'S LOW-MASS SATELLITES. Astron. J. *147*, 8. https://doi.org/10.1088/0004-6256/147/1/8.
78. Rubincam, D.P., Chao, B.F., and Thomas, P.C. (1995). The Gravitational Field of Deimos. Icarus *114*, 63–67. https://doi.org/10.1006/ICAR.1995.1043.
79. Duxbury, T.C. (1989). The figure of Phobos. Icarus *78*, 169–180. https://doi.org/10.1016/0019-1035(89)90075-4.
80. Ramsley, K.R., and Head, J.W. (2021). The Origins and Geological Histories of Deimos and Phobos: Hypotheses and Open Questions. Space Sci. Rev. *217*, 86. https://doi.org/10.1007/S11214-021-00864-1/FIGURES/12.
81. Tolson, R.H., Duxbury, T.C., Born, G.H., Christensen, E.J., Diehl, R.E., Farless, D., Hildebrand, C.E., Mitchell, R.T., Molko, P.M., Morabito, L.A., et al. (1978). Viking First Encounter of Phobos: Preliminary Results. Science *199*, 61–64. https://doi.org/10.1126/SCIENCE.199.4324.61.
82. Pang, K.D., Rhoads, J.W., Hanover, G.A., Lumme, K., and Bowell, E. (1983). Interpretation of whole-disk photometry of Phobos and Deimos. J. Geophys. Res. *88*, 2475–2484. https://doi.org/10.1029/JB088IB03P02475.

83. Thomas, P.C., Adinolfi, D., Helfenstein, P., Simonelli, D., and Veverka, J. (1996). The Surface of Deimos: Contribution of Materials and Processes to Its Unique Appearance. Icarus *123*, 536–556. https://doi.org/10.1006/ICAR.1996.0177.
84. Fraeman, A.A., Murchie, S.L., Arvidson, R.E., Clark, R.N., Morris, R.V., Rivkin, A.S., and Vilas, F. (2014). Spectral absorptions on Phobos and Deimos in the visible/near infrared wavelengths and their compositional constraints. Icarus *229*, 196–205. https://doi.org/10.1016/J.ICARUS.2013.11.021.
85. Murchie, S., Eng, D., Chabot, N., Guo, Y., Arvidson, R., Yen, A., Trebi-Ollennu, A., Seelos, F., Adams, E., and Fountain, G. (2014). MERLIN: Mars-Moon Exploration, Reconnaissance and Landed Investigation. Acta Astronaut. *93*, 475–482. https://doi.org/10.1016/J.ACTAASTRO.2012.10.014.
86. Hunten, D.M. (1979). Capture of Phobos and Deimos by photoatmospheric drag. Icarus *37*, 113–123. https://doi.org/10.1016/0019-1035(79)90119-2.
87. Rosenblatt, P., and Rosenblatt, P. (2011). The origin of the Martian moons revisited. Astron. AstroPhys. Rev. *19*, 1–26. https://doi.org/10.1007/S00159-011-0044-6.
88. Ronnet, T., Vernazza, P., and Mousis, O. (2016). The composition of the Martian moons Phobos and Deimos in a giant impact scenario. In 47th Lunar and Planetary Science Conference (USRA), p. 1941.
89. Citron, R.I., Genda, H., and Ida, S. (2015). Formation of Phobos and Deimos via a giant impact. Icarus *252*, 334–338. https://doi.org/10.1016/J.ICARUS.2015.02.011.
90. Hyodo, R., Genda, H., Charnoz, S., and Rosenblatt, P. (2017). On the Impact Origin of Phobos and Deimos. I. Thermodynamic and Physical Aspects. Astrophys. J. *845*, 125. https://doi.org/10.3847/1538-4357/AA81C4.
91. Takir, D., Matsuoka, M., Waiters, A., Kaluna, H., and Usui, T. (2022). Observations of Phobos and Deimos with SpeX at NASA infrared telescope facility. Icarus *371*, 114691. https://doi.org/10.1016/J.ICARUS.2021.114691.
92. Pang, K.D., Pollack, J.B., Veverka, J., Lane, A.L., and Ajello, J.M. (1978). The Composition of Phobos: Evidence for Carbonaceous Chondrite Surface from Spectral Analysis. Science *199*, 64–66. https://doi.org/10.1126/SCIENCE.199.4324.64.
93. Leone, G., Tackley, P.J., Gerya, T.V., May, D.A., and Zhu, G. (2014). Three-dimensional simulations of the southern polar giant impact hypothesis for the origin of the martian dichotomy. Geophys. Res. Lett. *41*, 8736–8743. https://doi.org/10.1002/2014GL062261.
94. Leone, G. (2016). Alignments of volcanic features in the southern hemisphere of Mars produced by migrating mantle plumes. J. Volcanol. Geotherm. Res. *309*, 78–95. https://doi.org/10.1016/j.jvolgeores.2015.10.028.
95. Hyodo, R., Rosenblatt, P., Genda, H., and Charnoz, S. (2017). On the Impact Origin of Phobos and Deimos. II. True Polar Wander and Disk Evolution. Astrophys. J. *851*, 122. https://doi.org/10.3847/1538-4357/AA9984.
96. Xian, S., Konrad, W., Jürgen, O., JinSong, P., and Shuhua, Y. (2012). Working models for the gravitational field of Phobos. Sci. China Physics, Mech. Astron. *552*, 358–364. https://doi.org/10.1007/S11433-011-4606-4.
97. Craddock, R.A. (2011). Are Phobos and Deimos the result of a giant impact? Icarus *211*, 1150–1161. https://doi.org/10.1016/J.ICARUS.2010.10.023.
98. Hesselbrock, A.J., and Minton, D.A. (2017). An ongoing satellite–ring cycle of Mars and the origins of Phobos and Deimos. Nat. Geosci. *10*, 266–269. https://doi.org/10.1038/ngeo2916.
99. Bagheri, A., Khan, A., Efroimsky, M., Kruglyakov, M., and Giardini, D. (2021). Dynamical evidence for Phobos and Deimos as remnants of a disrupted common progenitor. Nat. Astron. *5*, 539–543. https://doi.org/10.1038/s41550-021-01306-2.
100. Lunine, J.I., Neugebauer, G., and Jakosky, B.M. (1982). Infrared observations of Phobos and Deimos from Viking. J. Geophys. Res. *87*, 10297–10305. https://doi.org/10.1029/JB087IB12P10297.
101. Murchie, S.L., Britt, D.T., and Pieters, C.M. (2014). The value of Phobos sample return. Planet. Space Sci. *102*, 176–182. https://doi.org/10.1016/J.PSS.2014.04.014.
102. Usui, T., Bajo, K.i., Fujiya, W., Furukawa, Y., Koike, M., Miura, Y.N., Sugahara, H., Tachibana, S., Takano, Y., and Kuramoto, K. (2020). The Importance of Phobos Sample Return for Understanding the Mars-Moon System. Space Sci. Rev. *216*, 49. https://doi.org/10.1007/S11214-020-00668-9/TABLES/2.
103. Ferri, A., Pelle, S., Belluco, M., Voirin, T., and Gelmi, R. (2018). The exploration of PHOBOS: Design of a Sample Return mission. Adv. Space Res. *62*, 2163–2173. https://doi.org/10.1016/J.ASR.2018.06.014.
104. Kührt, E., and Giese, B. (1989). A thermal model of the Martian satellites. Icarus *81*, 102–112. https://doi.org/10.1016/0019-1035(89)90128-0.
105. Giese, B., and Kührt, E. (1990). Theoretical interpretation of infrared measurements at Deimos in the framework of crater radiation. Icarus *88*, 372–379. https://doi.org/10.1016/0019-1035(90)90088-Q.
106. Neugebauer, G., Münch, G., Chase, S.C., Hatzenbeler, H., Miner, E., and Schofield, D. (1969). Mariner 1969: Preliminary Results of the Infrared Radiometer Experiment. Science *166*, 98–99. https://doi.org/10.1126/SCIENCE.166.3901.98.
107. Neugebauer, G., Miinch, G., Kieffer, H., Chase, S.C.J., and Miner, E. (1971). Mariner 1969 Infrared Radiometer Results: Temperatures and Thermal Properties of the Martian Surface. Astron. J. *76*, 719. https://doi.org/10.1086/111189.
108. Kieffer, H.H., Chase, S.C., Miner, E., Münch, G., and Neugebauer, G. (1973). Preliminary report on infrared radiometric measurements from the Mariner 9 spacecraft. J. Geophys. Res. *78*, 4291–4312. https://doi.org/10.1029/JB078I020P04291.
109. Gatley, I., Kieffer, H., Miner, E., and Neugebauer, G. (1974). INFRARED OBSERVATIONS OF PHOBOS FROM MARINER 9. Astrophys. J. *4*, 497–503.
110. Kieffer, H.H., Martin, T.Z., Peterfreund, A.R., Jakosky, B.M., Miner, E.D., and Palluconi, F.D. (1977). Thermal and albedo mapping of Mars during the Viking primary mission. J. Geophys. Res. *82*, 4249–4291. https://doi.org/10.1029/JS082I028P04249.
111. Duxbury, T.C., and Veverka, J. (1977). Viking imaging of Phobos and Deimos: An overview of the primary mission. J. Geophys. Res. *82*, 4203–4211. https://doi.org/10.1029/JS082I028P04203.
112. Winter, D.F., and Saari, J.M. (1969). A particulate thermophysical model of the lunar soil. Astrophys. J. *156*, 1135–1151.
113. Linsky, J.L. (1966). Models of the lunar surface including temperature-dependent thermal properties. Icarus *5*, 606–634. https://doi.org/10.1016/0019-1035(66)90075-3.
114. Oze, C., and Sharma, M. (2007). Serpentinization and the inorganic synthesis of H2in planetary surfaces. Icarus *186*, 557–561. https://doi.org/10.1016/j.icarus.2006.09.012.
115. Stopar, J.D., Jeffrey Taylor, G., Hamilton, V.E., and Browning, L. (2006). Kinetic model of olivine dissolution and extent of aqueous alteration on mars. Geochim. Cosmochim. Acta *70*, 6136–6152. https://doi.org/10.1016/j.gca.2006.07.039.
116. Cartwright, R.J., Emery, J.P., Grundy, W.M., Cruikshank, D.P., Beddingfield, C.B., and Pinilla-Alonso, N. (2020). Probing the regoliths of the classical Uranian satellites: Are their surfaces mantled by a layer of tiny H2O ice grains? Icarus *338*, 113513. https://doi.org/10.1016/J.ICARUS.2019.113513.
117. Hanel, R., Conrath, B., Flasar, F.M., Kunde, V., Maguire, W., Pearl, J., Pirraglia, J., Samuelson, R., Cruikshank, D., Gautier, D., et al. (1986). Infrared Observations of the Uranian System. Science *233*, 70–74. https://doi.org/10.1126/SCIENCE.233.4759.70.
118. Schenk, P.M., and Moore, J.M. (2020). Topography and geology of Uranian mid-sized icy satellites in comparison with Saturnian and Plutonian satellites. Philos. Trans. R. Soc. A *378*, 20200102. https://doi.org/10.1098/RSTA.2020.0102.
119. Thomas, P.C., Parker, J.W., McFadden, L.A., Russell, C.T., Stern, S.A., Sykes, M.V., and Young, E.F. (2005). Differentiation of the asteroid Ceres as revealed by its shape. Nat *437*, 224–226. https://doi.org/10.1038/nature03938.
120. Park, R.S., Konopliv, A.S., Bills, B.G., Rambaux, N., Castillo-Rogez, J.C., Raymond, C.A., Vaughan, A.T., Ermakov, A.I., Zuber, M.T., Fu, R.R., et al. (2016). A partially differentiated interior for (1) Ceres deduced from its gravity field and shape. Nat *537*, 515–517. https://doi.org/10.1038/nature18955.
121. King, S.D., Castillo-Rogez, J.C., Toplis, M.J., Bland, M.T., Raymond, C.A., and Russell, C.T. (2018). Ceres internal structure from geophysical constraints. Meteorit. Planet. Sci. *53*, 1999–2007. https://doi.org/10.1111/MAPS.13063.
122. Fu, R.R., Ermakov, A.I., Marchi, S., Castillo-Rogez, J.C., Raymond, C.A., Hager, B.H., Zuber, M.T., King, S.D., Bland, M.T., Cristina De Sanctis, M., et al. (2017). The interior structure of Ceres as revealed by surface topography. Earth Planet Sci. Lett. *476*, 153–164. https://doi.org/10.1016/J.EPSL.2017.07.053.
123. Milliken, R.E., and Rivkin, A.S. (2009). Brucite and carbonate assemblages from altered olivine-rich materials on Ceres. Nat. Geosci. *2*, 258–261. https://doi.org/10.1038/ngeo478.
124. McCord, T.B., Combe, J.-P., Castillo-Rogez, J.C., McSween, H.Y., and Prettyman, T.H. (2022). Ceres, a wet planet: The view after Dawn. Geochemistry *82*, 125745. https://doi.org/10.1016/J.CHEMER.2021.125745.

125. Ammannito, E., Desanctis, M.C., Ciarniello, M., Frigeri, A., Carrozzo, F.G., Combe, J.P., Ehlmann, B.L., Marchi, S., McSween, H.Y., Raponi, A., et al. (2016). Distribution of phyllosilicates on the surface of Ceres. Science *353*, 353. https://doi.org/10.1126/SCIENCE.AAF4279/ASSET/6B62CB15-C2B1-4A9A-8E7F-07721C86585B/ASSETS/GRAPHIC/353_AAF4279_FA.JPEG.
126. Krohn, K., von der Gathen, I., Buczkowski, D.L., Jaumann, R., Wickhusen, K., Schulzeck, F., Stephan, K., Wagner, R., Scully, J.E.C., Raymond, C.A., and Russell, C. (2020). Fracture geometry and statistics of Ceres' floor fractures. Planet. Space Sci. *187*, 104955. https://doi.org/10.1016/J.PSS.2020.104955.
127. Buczkowski, D.L., Sizemore, H.G., Bland, M.T., Scully, J.E.C., Quick, L.C., Hughson, K.H.G., Park, R.S., Preusker, F., Raymond, C.A., and Russell, C.T. (2018). Floor-Fractured Craters on Ceres and Implications for Interior Processes. JGR. Planets *123*, 3188–3204. https://doi.org/10.1029/2018JE005632.
128. Hall, J.L., Solomon, S.C., and Head, J.W. (1981). Lunar floor-fractured craters: Evidence for viscous relaxation of crater topography. J. Geophys. Res. *86*, 9537–9552. https://doi.org/10.1029/JB086IB10P09537.
129. Schultz, P.H. (1976). Floor-fractured lunar craters. Moon *15*, 241–273. https://doi.org/10.1007/BF00562240.
130. Jozwiak, L.M., Head, J.W., Zuber, M.T., Smith, D.E., and Neumann, G.A. (2012). Lunar floor-fractured craters: Classification, distribution, origin and implications for magmatism and shallow crustal structure. J. Geophys. Res. *117*, 11005. https://doi.org/10.1029/2012JE004134.
131. Jozwiak, L.M., Head, J.W., and Wilson, L. (2015). Lunar floor-fractured craters as magmatic intrusions: Geometry, modes of emplacement, associated tectonic and volcanic features, and implications for gravity anomalies. Icarus *248*, 424–447. https://doi.org/10.1016/J.ICARUS.2014.10.052.
132. Jozwiak, L.M., Head III, J., Neumann, G.A., and Wilson, L. (2017). Observational constraints on the identification of shallow lunar magmatism: Insights from floor-fractured craters. Icarus *283*, 224–231. https://doi.org/10.1016/J.ICARUS.2016.04.020.
133. Thorey, C., and Michaut, C. (2014). A model for the dynamics of crater-centered intrusion: Application to lunar floor-fractured craters. JGR. Planets *119*, 286–312. https://doi.org/10.1002/2013JE004467.
134. Bamberg, M., Jaumann, R., Asche, H., Kneissl, T., and Michael, G.G. (2014). Floor-Fractured Craters on Mars – Observations and Origin. Planet. Space Sci. *98*, 146–162. https://doi.org/10.1016/J.PSS.2013.09.017.
135. Leone, G. (2017). Mangala Valles, Mars: A reassessment of formation processes based on a new geomorphological and stratigraphic analysis of the geological units. J. Volcanol. Geotherm. Res. *337*, 62–80. https://doi.org/10.1016/j.jvolgeores.2017.03.011.
136. Wichman, R.W., and Schultz, P.H. (1995). Floor-fractured impact craters on Venus: Implications for igneous crater modification and local magmatism. J. Geophys. Res. *100*, 3233–3244. https://doi.org/10.1029/94JE03206.
137. Wichman, R.W., and Schultz, P.H. (1995). Floor-fractured craters in Mare Smythii and west of Oceanus Procellarum: Implications of crater modification by viscous relaxation and igneous intrusion models. J. Geophys. Res. *100*, 21201–21218. https://doi.org/10.1029/95JE02297.
138. Dombard, A.J., and Gillis, J.J. (2001). Testing the viability of topographic relaxation as a mechanism for the formation of lunar floor-fractured craters. J. Geophys. Res. *106*, 27901–27909. https://doi.org/10.1029/2000JE001388.
139. Oze, C., and Sharma, M. (2005). Have olivine, will gas: Serpentinization and the abiogenic production of methane on Mars. Geophys. Res. Lett. *32*, L10203. https://doi.org/10.1029/2005GL022691.
140. Neveu, M., and Desch, S.J. (2015). Geochemistry, thermal evolution, and cryovolcanism on Ceres with a muddy ice mantle. Geophys. Res. Lett. *42*, 197–210. https://doi.org/10.1002/2015GL066375.
141. Castillo-Rogez, J.C., and McCord, T.B. (2010). Ceres' evolution and present state constrained by shape data. Icarus *205*, 443–459. https://doi.org/10.1016/J.ICARUS.2009.04.008.
142. McCord, T.B., and Sotin, C. (2005). Ceres: Evolution and current state. J. Geophys. Res. *110*, 1–14. https://doi.org/10.1029/2004JE002244.
143. Kurokawa, H., Ehlmann, B.L., De Sanctis, M.C., Lapôtre, M.G.A., Usui, T., Stein, N.T., Prettyman, T.H., Raponi, A., and Ciarniello, M. (2020). A Probabilistic Approach to Determination of Ceres' Average Surface Composition From Dawn Visible-Infrared Mapping Spectrometer and Gamma Ray and Neutron Detector Data. JGR. Planets *125*, e2020JE006606. https://doi.org/10.1029/2020JE006606.
144. Marchi, S., Raponi, A., Prettyman, T.H., De Sanctis, M.C., Castillo-Rogez, J., Raymond, C.A., Ammannito, E., Bowling, T., Ciarniello, M., Kaplan, H., et al. (2018). An aqueously altered carbon-rich Ceres. Nat. Astron. *3*, 140–145. https://doi.org/10.1038/s41550-018-0656-0.
145. Sori, M.M., Byrne, S., Bland, M.T., Bramson, A.M., Ermakov, A.I., Hamilton, C.W., Otto, K.A., Ruesch, O., and Russell, C.T. (2017). The vanishing cryovolcanoes of Ceres. Geophys. Res. Lett. *44*, 1243–1250. https://doi.org/10.1002/2016GL072319.
146. Lockwood, A.C., Brown, M.E., and Stansberry, J. (2014). The Size and Shape of the Oblong Dwarf Planet Haumea. Earth Moon Planets *111*, 127–137. https://doi.org/10.1007/S11038-014-9430-1.
147. Ortiz, J.L., Santos-Sanz, P., Sicardy, B., Benedetti-Rossi, G., Bérard, D., Morales, N., Duffard, R., Braga-Ribas, F., Hopp, U., Ries, C., et al. (2017). The size, shape, density and ring of the dwarf planet Haumea from a stellar occultation. Nat *550*, 219–223. https://doi.org/10.1038/nature24051.
148. Dunham, E.T., Desch, S.J., and Probst, L. (2019). Haumea's Shape, Composition, and Internal Structure. Astrophys. J. *877*, 41. https://doi.org/10.3847/1538-4357/AB13B3.
149. Schaller, E.L., and Brown, M.E. (2008). Detection of Additional Members of the 2003 EL61 Collisional Family via Near-Infrared Spectroscopy. Astrophys. J. *684*, L107–L109. https://doi.org/10.1086/592232/FULLTEXT/.
150. Levison, H.F., Morbidelli, A., Vokrouhlický, D., and Bottke, W.F. (2008). ON A SCATTERED-DISK ORIGIN FOR THE 2003 EL61 COLLISIONAL FAMILY—AN EXAMPLE OF THE IMPORTANCE OF COLLISIONS ON THE DYNAMICS OF SMALL BODIES. Astron. J. *136*, 1079–1088. https://doi.org/10.1088/0004-6256/136/3/1079.
151. Marcus, R.A., Ragozzine, D., Murray-Clay, R.A., and Holman, M.J. (2011). IDENTIFYING COLLISIONAL FAMILIES IN THE KUIPER BELT. Astrophys. J. *733*, 40. https://doi.org/10.1088/0004-637X/733/1/40.
152. Vilenius, E., Stansberry, J., Müller, T., Mueller, M., Kiss, C., Santos-Sanz, P., Mommert, M., Pál, A., Lellouch, E., Ortiz, J.L., et al. (2018). "TNOs are Cool": A survey of the trans-Neptunian region - XIV. Size/albedo characterization of the Haumea family observed with Herschel and Spitzer. Astron. Astrophys. *618*, A136. https://doi.org/10.1051/0004-6361/201732564.
153. Brown, M.E., Barkume, K.M., Ragozzine, D., and Schaller, E.L. (2007). A collisional family of icy objects in the Kuiper belt. Nat *446*, 294–296. https://doi.org/10.1038/nature05619.
154. Leinhardt, Z.M., Marcus, R.A., and Stewart, S.T. (2010). THE FORMATION OF THE COLLISIONAL FAMILY AROUND THE DWARF PLANET HAUMEA. Astrophys. J. *714*, 1789–1799. https://doi.org/10.1088/0004-637X/714/2/1789.
155. Ragozzine, D., and Brown, M.E. (2007). Candidate Members and Age Estimate of the Family of Kuiper Belt Object 2003 EL61. Astron. J. *134*, 2160–2167. https://doi.org/10.1086/522334/FULLTEXT/.
156. Pinilla-Alonso, N., Licandro, J., and Lorenzi, V. (2008). Visible spectroscopy in the neighborhood of 2003EL61. Astron. Astrophys. *489*, 455–458. https://doi.org/10.1051/0004-6361:200810226.
157. Stansberry, J.A., Grundy, W.M., Mueller, M., Benecchi, S.D., Rieke, G.H., Noll, K.S., Buie, M.W., Levison, H.F., Porter, S.B., and Roe, H.G. (2012). Physical properties of trans-neptunian binaries (120347) Salacia–Actaea and (42355) Typhon–Echidna. Icarus *219*, 676–688. https://doi.org/10.1016/J.ICARUS.2012.03.029.
158. Fernández-Valenzuela, E., Pinilla-Alonso, N., Stansberry, J., Emery, J.P., Perkins, W., Van Laerhoven, C., Gladman, B.J., Fraser, W., Cruikshank, D., Lellouch, E., et al. (2021). Compositional Study of Trans-Neptunian Objects at $\lambda > 2.2$ μm. Planet. Sci. J. *2*, 10. https://doi.org/10.3847/PSJ/ABC34E.
159. Grundy, W.M., Noll, K.S., Nimmo, F., Roe, H.G., Buie, M.W., Porter, S.B., Benecchi, S.D., Stephens, D.C., Levison, H.F., and Stansberry, J.A. (2011). Five new and three improved mutual orbits of transneptunian binaries. Icarus *213*, 678–692. https://doi.org/10.1016/J.ICARUS.2011.03.012.
160. Galiazzo, M., de la Fuente Marcos, C., de la Fuente Marcos, R., Carraro, G., Maris, M., and Montalto, M. (2016). Photometry of Centaurs and trans-Neptunian objects: 2060 Chiron (1977 UB), 10199 Chariklo (1997 CU26), 38628 Huya (2000 EB173), 28978 Ixion (2001 KX76), and 90482 Orcus (2004 DW). Astrophys. Space Sci. *361*, 1–15. https://doi.org/10.1007/S10509-016-2801-5/TABLES/18.
161. Barucci, M.A., Merlin, F., Guilbert, A., de Bergh, C., Alvarez-Candal, A., Hainaut, O.,

Doressoundiram, A., Dumas, C., Owen, T., and Coradini, A. (2008). Surface composition and temperature of the TNO Orcus. Astron. Astrophys. *479*, L13–L16. https://doi.org/10.1051/0004-6361:20079079.

162. Brown, M.E., Ragozzine, D., Stansberry, J., and Fraser, W.C. (2010). THE SIZE, DENSITY, AND FORMATION OF THE ORCUS–VANTH SYSTEM IN THE KUIPER BELT. Astron. J. *139*, 2700–2705. https://doi.org/10.1088/0004-6256/139/6/2700.
163. Lim, T.L., Stansberry, J., Müller, T.G., Mueller, M., Lellouch, E., Kiss, C., Santos-Sanz, P., Vilenius, E., Protopapa, S., Moreno, R., et al. (2010). "TNOs are Cool": A survey of the trans-Neptunian region - III. Thermophysical properties of 90482 Orcus and 136472 Makemake. Astron. Astrophys. *518*, L148. https://doi.org/10.1051/0004-6361/201014701.
164. Carry, B., Hestroffer, D., Demeo, F.E., Thirouin, A., Berthier, J., Lacerda, P., Sicardy, B., Doressoundiram, A., Dumas, C., Farrelly, D., and Müller, T.G. (2011). Integral-field spectroscopy of (90482) Orcus-Vanth. Astron. Astrophys. *534*, A115. https://doi.org/10.1051/0004-6361/201117486.
165. Sickafoose, A.A., Bosh, A.S., Levine, S.E., Zuluaga, C.A., Genade, A., Schindler, K., Lister, T.A., and Person, M.J. (2019). A stellar occultation by Vanth, a satellite of (90482) Orcus. Icarus *319*, 657–668. https://doi.org/10.1016/J.ICARUS.2018.10.016.
166. Fornasier, S., Lellouch, E., Müller, T., Santos-Sanz, P., Panuzzo, P., Kiss, C., Lim, T., Mommert, M., Bockelée-Morvan, D., Vilenius, E., et al. (2013). TNOs are Cool: A survey of the trans-Neptunian region. Astron. Astrophys. *555*, A15. https://doi.org/10.1051/0004-6361/201321329.
167. Delsanti, A., Merlin, F., Guilbert-Lepoutre, A., Bauer, J., Yang, B., and Meech, K.J. (2010). Methane, ammonia, and their irradiation products at the surface of an intermediate-size KBO? - A portrait of Plutino (90482) Orcus. Astron. Astrophys. *520*, A40. https://doi.org/10.1051/0004-6361/201014296.
168. Dalle Ore, C.M., Barucci, M.A., Emery, J.P., Cruikshank, D.P., Dalle Ore, L.V., Merlin, F., Alvarez-Candal, A., De Bergh, C., Trilling, D.E., Perna, D., et al. (2009). Composition of KBO (50000) Quaoar. Astron. Astrophys. *501*, 349–357. https://doi.org/10.1051/0004-6361/200911752.
169. Fraser, W.C., and Brown, M.E. (2010). QUAOAR: A ROCK IN THE KUIPER BELT. Astrophys. J. *714*, 1547–1550. https://doi.org/10.1088/0004-637X/714/2/1547.
170. Braga-Ribas, F., Sicardy, B., Ortiz, J.L., Lellouch, E., Tancredi, G., Lecacheux, J., Vieira-Martins, R., Camargo, J.I.B., Assafin, M., Behrend, R., et al. (2013). THE SIZE, SHAPE, ALBEDO, DENSITY, AND ATMOSPHERIC LIMIT OF TRANSNEPTUNIAN OBJECT (50000) QUAOAR FROM MULTI-CHORD STELLAR OCCULTATIONS. Astrophys. J. *773*, 26. https://doi.org/10.1088/0004-637X/773/1/26.
171. Brown, M.E., and Trujillo, C.A. (2004). Direct Measurement of the Size of the Large Kuiper Belt Object (50000) Quaoar. Astron. J. *127*, 2413–2417. https://doi.org/10.1086/382513/FULLTEXT/.
172. Fraser, W.C., Batygin, K., Brown, M.E., and Bouchez, A. (2013). The mass, orbit, and tidal evolution of the Quaoar–Weywot system. Icarus *222*, 357–363. https://doi.org/10.1016/J.ICARUS.2012.11.004.
173. Barr, A.C., and Schwamb, M.E. (2016). Interpreting the densities of the Kuiper belt's dwarf planets. Mon. Not. R. Astron. Soc. *460*, 1542–1548. https://doi.org/10.1093/MNRAS/STW1052.
174. Barucci, M.A., Ore, C.M.D., Alvarez-Candal, A., Bergh, C. de, Merlin, F., Dumas, C., and Cruikshank, D. (2010). SEDNA: INVESTIGATION OF SURFACE COMPOSITIONAL VARIATION. Astron. J. *140*, 90377. 2095. https://doi.org/10.1088/0004-6256/140/6/2095.
175. Gladman, B., Marsden, B.G., and VanLaerhoven, C. (2008). Nomenclature in the Outer Solar System. In The Solar System Beyond Neptune (University of Arizona Press)), pp. 43–57.
176. Hussmann, H., Sohl, F., and Spohn, T. (2006). Subsurface oceans and deep interiors of medium-sized outer planet satellites and large trans-neptunian objects. Icarus *185*, 258–273. https://doi.org/10.1016/J.ICARUS.2006.06.005.
177. Emery, J.P., Dalle Ore, C.M., Cruikshank, D.P., Fernández, Y.R., Trilling, D.E., and Stansberry, J.A. (2007). Ices on (90377) Sedna: confirmation and compositional constraints. Astron. Astrophys. *466*, 395–398. https://doi.org/10.1051/0004-6361:20067021.
178. Barucci, M.A., Cruikshank, D.P., Dotto, E., Merlin, F., Poulet, F., Dalle Ore, C., Fornasier, S., and de Bergh, C. (2005). Is Sedna another Triton? Astron. Astrophys. *439*, L1–L4. https://doi.org/10.1051/0004-6361:200500144.
179. Cruikshank, D.P. (2005). Triton, Pluto, Centaurs, and Trans-Neptunian Bodies. Space Sci. Rev. 421–439. https://doi.org/10.1007/S11214-005-1964-0.
180. Cruikshank, D.P., Roush, T.L., Bartholomew, M.J., Geballe, T.R., Pendleton, Y.J., White, S.M., Bell, J.F., Davies, J.K., Owen, T.C., De Bergh, C., et al. (1998). The Composition of Centaur 5145 Pholus. Icarus *135*, 389–407. https://doi.org/10.1006/ICAR.1998.5997.
181. de Koker, N.P., Stixrude, L., and Karki, B.B. (2008). Thermodynamics, structure, dynamics, and freezing of Mg2SiO4 liquid at high pressure. Geochim. Cosmochim. Acta *72*, 1427–1441. https://doi.org/10.1016/J.GCA.2007.12.019.
182. Davoisne, C., Djouadi, Z., Leroux, H., D'Hendecourt, L., Jones, A., and Deboffle, D. (2006). The origin of GEMS in IDPs as deduced from microstructural evolution of amorphous silicates with annealing. Astron. Astrophys. *448*, L1–L4. https://doi.org/10.1051/0004-6361:200600002.
183. Rhoden, A.R., and Walker, M.E. (2022). The case for an ocean-bearing Mimas from tidal heating analysis. Icarus *376*, 114872. https://doi.org/10.1016/J.ICARUS.2021.114872.
184. Neveu, M., and Rhoden, A.R. (2017). The origin and evolution of a differentiated Mimas. Icarus *296*, 183–196. https://doi.org/10.1016/j.icarus.2017.06.011.
185. Hildenbrand, G., Paschek, K., Schäfer, M., Hausmann, M., Hildenbrand, G., Paschek, K., Schäfer, M., and Hausmann, M. (2022). In Cryovolcanism in the Solar System and Beyond: Considerations on Energy Sources, Geological Aspects, and Astrobiological Perspectives, Y.H. Chemin, ed. (IntechOpen). Astronomy. https://doi.org/10.5772/INTECHOPEN.105067.
186. Leone, G., Grosse, P., Ahrens, C., and Gasparri, D. (2022). Geomorphological and morphometric characteristics of the volcanic edifices along a volcanic alignment of Tharsis on Mars. Geomorphology *414*, 108385. https://doi.org/10.1016/J.GEOMORPH.2022.108385.
187. Raymond, S.N., O'Brien, D.P., Morbidelli, A., and Kaib, N.A. (2009). Building the terrestrial planets: Constrained accretion in the inner Solar System. Icarus *203*, 644–662. https://doi.org/10.1016/j.icarus.2009.05.016.
188. Margot, J.-L. (2015). A QUANTITATIVE CRITERION FOR DEFINING PLANETS. Astron. J. *150*, 185. https://doi.org/10.1088/0004-6256/150/6/185.